A New Method for Detecting Urban Morphology Effects on Urban-scale Air Temperature and Building Energy Consumption under Mesoscale Meteorological Conditions

Ruiqing Du [a], Chun-Ho Liu [a, *], and Xian-Xiang Li [b, c, d]

[a] *Department of Mechanical Engineering, The University of Hong Kong, Hong Kong*
[b] *School of Atmospheric Sciences, Sun Yat-sen University, China*
[c] *Key Laboratory of Tropical Atmosphere-Ocean System, Ministry of Education, China*
[d] *Southern Marine Science and Engineering Guangdong Laboratory (Zhuhai), China*

Manuscript submitted
to
Urban Climates
on
June 6, 2023

**Correspondence:*
Dr. Chun-Ho LIU

Department of Mechanical Engineering,
The University of Hong Kong,
Pokfulam Road, Hong Kong SAR, CHINA

Tel: +852 3917 7901 / + 852 9788 7951
Fax: +852 2858 5415
liuchunho@graduate.hku.hk
https://aplhk.tech
ORCID: 0000-0002-4609-524X

Abstract

Impact of urban morphology on urban-scale building energy consumption under mesoscale climate has not been elucidated. A new model was developed to examine the impact using the mesoscale Weather Research and Forecasting (WRF) model. For the first time, local climate zone and building categories (LCZBCs) are integrated into WRF, handling landuse/landcover and building configuration. The urban morphology parameters are clustered into three groups: urban structure, vegetation fraction, and impervious surface thermal properties. Our results show that urban structure induces a higher urban heat island (UHI) intensity at nighttime than does in daytime. The difference in urban-rural building/street structure is the key factor in compact and open high-rise areas, especially commercial-dominant ones, where the UHI intensity and AC load are increased by 40.33% and 34.52%, respectively. Besides, greenery is most effective to mitigate UHI problems, lessening AC demand in middle-rise and low-rise areas. Its benefit is most prominent for residential-dominant areas that could reduce the UHI intensity and AC load as much as 106.26% and 53.13%, respectively. In contrast to rural pavement, urban impervious surfaces induce negligible increases in temperature (4.75%) and AC load (2.33%). The outcome provides insights into the dominant parameters in LCZBCs and the strategy for urban (re)development. (200 words)

Keywords: air-conditioning (AC) load; building category; building energy consumption; energy policy; local climate zone (LCZ); urban heat island (UHI); urban morphology

Abbreviation	
AC	Air-conditioning
AR	Mean height-to-width ratio of street canyons (LCZ1–6) or building spacing (LCZ8–10)
BEP	Building effect parameterization
BEM	Building energy model
BSF	Building surface fraction
ISA	Impervious surface albedo
ISHC	Impervious surface heat capacity
ISTD	Impervious surface thermal conductivity
LCZ	Local climate zone
LULC	Landuse and landcover
SVF	Sky view factor
UHI	Urban heat island
UHII	Urban heat island intensity
UMP	Urban morphology parameter
VF	Vegetation fraction
WRF	Weather Research and Forecasting
WUDAPT	World Urban Database and Access Portal Tools
Mathematical Symbol	
ΔACE	Difference in air-conditioning electricity
$\Delta ISTP$	Difference in the thermal properties of impervious surfaces
ΔSCD	Difference in sensible cooling demand
$\Delta T2$	Difference in urban heat island intensities
ΔVF	Difference in vegetation fraction
Subscript	
urban-rural	Comparison between urban and rural in real case
structure	Comparison between urban and rural structure
vf	Comparison between urban and rural vegetation fraction
is	Comparison of the thermal properties between urban and rural impervious surface

1. Introduction

Human-induced global warming has led to a significant rise in urban air temperature (Alcoforado & Andrade, 2008). Air-conditioning (AC) is one of the remedial measures in building indoor environment. However, tremendous electric load of AC (AC load) would pose huge, citywide energy requirement in summer. The peaked electricity demand surges especially during heatwave events. Latest studies have unveiled that AC-related energy consumption could be over 50% of the total in China (IEA, 2019) and the United States ("The Future of Cooling," 2018). It could even result in power grid failure (Stone Jr et al., 2021). Hong Kong (HK), a compact city with subtropical climate, has further intensified urban heat island (UHI; (Wang et al., 2021) and increased AC load (Shi et al., 2019). In summer, the peaked electricity demand could jump to 66% of the output (Lou et al., 2006). Therefore, unraveling the mechanism of intra-urban heterogeneity in temperature and energy demand is crucial to the effectuation of energy policy.

Among others, urban morphology is a key factor for urban climate and building energy consumption (Ishii et al., 2010). Its impact on microclimate was extensively studied for decades but was rather limited on building energy. By an extensive literature review, Quan and Li (2021) found that most studies had focused on the interaction between urban morphology and building energy consumption in microscale only. Whereas, it is well known fact that urban form could aggravate or mitigate the large-scale weather effect on building energy consumption especially in mesoscale (Allen-Dumas et al., 2020). In this connection, there is a pressing need for the advanced mechanism between microscale and mesoscale climate for urban-scale building energy models (BEMs) in the crisis of global warming.

Meteorological input is essential to reliable urban-scale BEMs that mainly bases on observation and simulation. Long-term anemometry monitoring data (years or decades) are commonly adopted to drive urban-scale BEMs (Assimakopoulos et al., 2007). They, however, are sparse geographically that merely differentiate the inhomogeneous urban climate nowadays especially in microscale. Weather simulation, on the other hand, enables refined spatio-temporal resolution of meteorological variables. Hence, integrating microclimate models into urban-scale BEMs is a workaround for practical problems. Microclimate models explicitly resolve building geometry to offer precise spatial results. Whereas, they are unable to handle mesoscale meteorological processes that overlooks a major component in building energy consumption. In contrast, mesoscale Weather Research and Forecasting (WRF) model, coupling urban canopy model (UCM) and BEM (Salamanca et al., 2010), enables urban-scale building energy analysis by considering the more realistic weather conditions and natural terrain. WRF-BEP/BEM model has been validated based on the Greater Tokyo (Kikegawa et al., 2014), Phoenix (Salamanca et al., 2013), Beijing (Xu et al., 2018), Bolzano (Pappaccogli et al., 2021), Osaka (Takane et al., 2017) and New York (Ortiz et al., 2017) for the prediction of AC energy demand. Thus, it could be used as a promising method to examine the effect of urban morphology on urban-scale air temperature and AC load considering multi-scale meteorology conditions.

High-resolution UMPs are critical to the accuracy of meteorology models (Stewart et al., 2014). To address urban-climate challenges, the project of World Urban Database Access Portal Tools (WUDAPT) comprised the information of urban form and function, classifying the landcover into 10 types of local climate zone (LCZ;

Stewart & Oke, 2012). It has been applied extensively that could improve the model performance of urban-climate simulation by representing microclimate in detail (Aslam & Rana, 2022).

To the best knowledge of the authors, however, the effect of urban morphology on urban-scale AC load under mesoscale meteorological conditions remains an open question. Besides, as city-scale BEM, previous WRF-BEP/BEM models have only used three categories (low-intensity residential, high-intensity residential, and industrial/commercial) in the urban morphology parameter (UMP) that would merely describe the complicated city setting nowadays. On the other hand, LCZ maps (with detailed UMPs) were rarely incorporated into mesoscale meteorology models for urban-scale building energy consumption because of the lack of building category in LCZ classification (Santos et al., 2020). Moreover, as an integrated landuse/landcover (LULC) classification, LCZ includes a range of UMPs such as sky view factors (SVFs), building surface fraction (BSF), and surface thermal properties. Previous studies have examined the relationship among LCZ, urban climate, and single-building energy consumption (Yang et al., 2020). Whereas, the influence of individual UMPs on urban climate and building energy consumption is unknown.

To bridge the aforementioned knowledge gap, we developed a new urban-scale BEM by sub-classifying and incorporating LCZ building categories (LCZBCs) into the multi-layer WRF-BEP/BEM model (WRF-LCZBC) for the first time. Using this model, the sensitivity of UHII and building energy consumption during a heatwave event in HK (June 23 to 28, 2016; Du et al., 2021) to UMPs was tested. Those UMPs available in LCZ classification (Stewart & Oke, 2012) are clustered into three groups: urban structure, vegetation fraction (VF), and impervious surface thermal properties in this study. Their contributions to intra-urban heterogeneity in urban climate and building energy consumption were isolated and compared. This model could be a new approach to determine the dominant parameter in each LCZBC type in favor of urban environment and urban-scale building energy demand. The outcome could help policymakers foster the most cost-effective strategy in urban design for sustainability.

2. Methodology

A new LULC configuration, which sub-classifies building categories based on LCZ classification (LCZBC) from WUDAPT, is developed. The LCZBC maps are integrated into a high-resolution WRF model (333 m) coupled with multi-layer UCM and BEM. The newly developed model is validated by the annual building energy consumption and the representative load curves (Pappaccogli et al., 2021). Three sensitivity tests are conducted by changing the urban structure, VF, and thermal properties of impervious surfaces to isolate UHII and additional AC load. The methodology part is organized as follows: Section 2.1 presents the basic information of the area concerned. Section 2.2 introduces the data sources and the LCZBC classification. The hourly AC load for validation is shown in Sections 2.3 and 2.4. The scenario and hypothesis are summarized in Section 2.5. Finally, the setting and configuration of WRF-BEP/BEM model are recorded in Section 2.6.

2.1 Geographical Area

HK is a dense, high-rise metropolis, locating in the southeastern coast of China (22 °N, 114 °E). It is characterized by its subtropical and Asian monsoon climate where is hot (30~35 °C) and wet (81~83% relative humidity; RH) in summer together with warm (18~21 °C) and humid (70~79% RH) in winter. The prevailing wind is southwesterly in summer and northeasterly in winter. The average wind speed is 5.0 m/s and 4.2 m/s, respectively, in windier season (September 30 to March 14) and calmer season (March 14 to September 30). The total area of HK is 1,064 km^2 in which 70% is hilly terrain. As a result, majority population (95% of 7.41 million lives in less than 20% of the land area, mainly residing in Kowloon Peninsula and the northern coast of HK Island along Victoria Harbor (HKCSD, 2021). In view of the dense urban setting, the Hong Kong public suffers from UHI-induced problems such as thermal stress and the subsequent health issues (HKPlanD, 2012). AC is commonly used to ease the thermal discomfort. It, however, ends up with a city-wide increase in energy demand that is more apparent in the current crisis of global warming. The building energy consumption for space cooling could be increased by 80% to 140% during extreme heatwave events (Morakinyo et al., 2019).

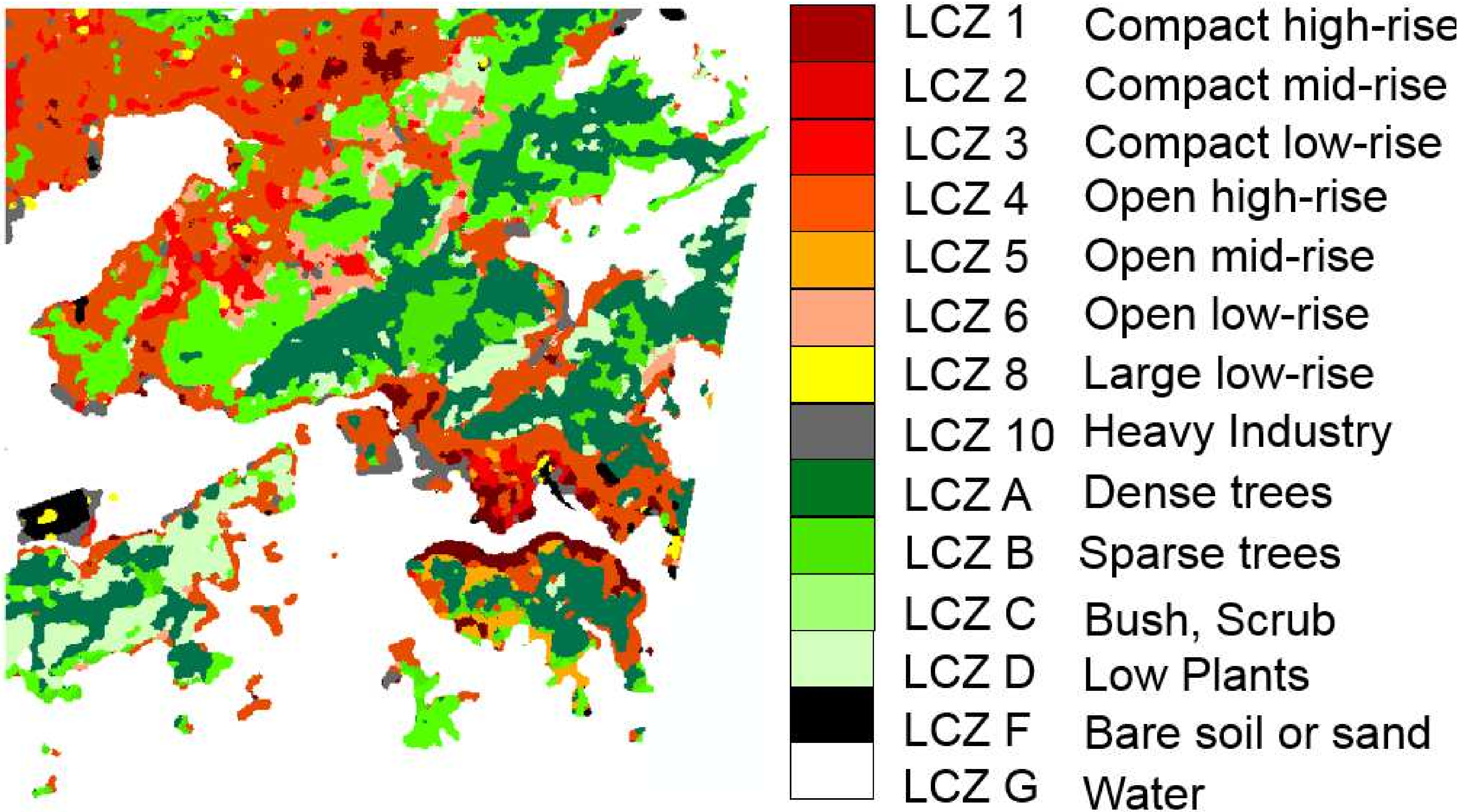

Figure 1. Map of local climate zones (LCZs) in HK (Wang et al., 2018).

2.2 Data

2.2.1 Urban Morphology

High-resolution (100 m) LCZ data collected from WUDAPT datasets (Wang et al., 2018) are used in this study to acquire UMPs. The LCZ scheme classifies LULC into 17 types according to surface configuration and material properties. Ten of them are urban (LCZ1-10) and the rest are natural terrain (LCZ A-G). In HK, the dominant urban LCZs are Open high-rise (LCZ4, 54.8%), Open mid-rise (LCZ5, 24.6%) and Compact high-rise (LCZ1, 8.7%; Figure 1). The LCZ parameters are integrated into the WRF model, describing the LULC (Section 2.6).

2.2.2 Building Classification

Diversified building categories in the same LCZ could induce heterogeneous building energy consumption that is not yet covered in terms of UMPs (Santos et al., 2020). As such, a sub-classification (LCZBC) is proposed by overlying building categories onto the readily available LCZ map (Table 1). The resolution of the new LULC map is also 100 m. In each of the 10 urban LCZ types, the landuse data are further categorized into three grades (commercial, residential, and non-building) according to the dominant LULC. In addition, the building-category information is used in this study for model evaluation (Section 2.4). It is extracted from the high-resolution (10 m) land utilization maps of the Planning Department (PlanD) of HK Special Administrative Region (HKSAR; HKPlanD, 2018). The building floor area in HK is estimated by geographic information system (GIS) based on fine-resolution urban maps.

Table 1. Sub-classification of local climate zones (LCZs) based on building category.

LCZ	Urban morphology	LCZBC	Building category	Area ratio[a] (%)	DC[b] (km)
LCZ1	Compact high-rise	LCZ1-C	Commercial	0.27	1.30
		LCZ1-R	Residential	0.34	1.36
		LCZ1-N	Non-building	1.19	2.30
LCZ2	Compact mid-rise	LCZ2-C	Commercial	0.08	1.95
		LCZ2-R	Residential	0.09	1.37
		LCZ2-N	Non-building	0.18	1.36
LCZ3	Compact low-rise	LCZ3-C	Commercial	0.18	2.05
		LCZ3-R	Residential	0.16	3.38
		LCZ3-N	Non-building	1.76	3.78
LCZ4	Open high-rise	LCZ4-C	Commercial	0.87	2.37
		LCZ4-R	Residential	1.21	2.94
		LCZ4-N	Non-building	14.29	2.87
LCZ5	Open mid-rise	LCZ5-C	Commercial	0.11	1.40
		LCZ5-R	Residential	0.16	1.28
		LCZ5-N	Non-building	0.47	1.50
LCZ6	Open low-rise	LCZ6-C	Commercial	0.10	2.59
		LCZ6-R	Residential	0.05	3.85
		LCZ6-N	Non-building	2.01	5.42
LCZ7	Lightweight low-rise	LCZ7-C	Commercial	0.00	1.81
		LCZ7-R	Residential	0.00	2.42
		LCZ7-N	Non-building	0.00	1.16
LCZ8	Large low-rise	LCZ8-C	Commercial	0.13	2.49
		LCZ8-R	Residential	0.00	1.64
		LCZ8-N	Non-building	0.19	1.30
LCZ9	Sparsely built	LCZ9-C	Commercial	0.00	1.36
		LCZ9-R	Residential	0.00	2.30
		LCZ9-N	Non-building	0.00	1.95
LCZ10	Heavy industry	LCZ10-C	Commercial	0.46	1.37
		LCZ10-R	Residential	0.03	1.36
		LCZ10-N	Non-building	1.07	2.05

Remark: [a] Area ratio: Ratio of the number of model grids of a specific LCZBC type to total number of model grids in Domain 4.

[b] DC: Average distance to coastline of all model grids of a specific LCZBC type in Domain 4.

2.2.3 Energy Utilization Index

The annual energy consumption of a range of (representative) buildings was monitored by the Electrical and Mechanical Services Department (EMSD) of HKSAR (EMSD, 2021). The dataset covers 2,595 buildings, especially those in dense, high-rise urban downtown. It records the electricity consumption of 4 types of facilities: elevator, lighting, AC, and electric installation of individual buildings. The electricity consumption is normalized as energy utilization index (EUI) which is the annual electricity consumption divided by the building floor area (kW hr m^{-2} yr^{-1}). The total EUI is multiplied by the building-category ratio (commercial: 62%, residential: 64%) collected from the EMSD statistics (HKEMSD, 2018) as well as previous studies (Jing et al., 2017) to obtain the AC load.

2.3 Energy Consumption Load Curve

For model evaluation, representative load curves for buildings are obtained from annual building energy consumption simulation. In this study, the hourly electricity consumption of commercial and residential buildings is calculated by Energyplus V8.9 (Crawley et al., 2000). Typical commercial and residential buildings are modeled in compliance with the guidelines of HKSAR Government ("Code of Practice for overall thermal transfer value in Buildings 1995," 1995) and the Standard Block Typical Floor Plans of HK Housing Authority (HKHA, 2021), respectively. The indoor temperature set-point is 25 ^{o}C. The occupancy density is 13 m^2/person, 10 m^2/person, and 12.5 m^2/person for offices, shopping malls, and residences, respectively. The simulation time-step increment is 10 min. More details, such as the operation schedule and the building envelope in the Energyplus simulation, were reported elsewhere (Huang & Niu, 2015; Yu et al., 2020). The 5-day average (curve) of the diurnal load profile during the analysis period (June 23 to 28, 2016; heatwave event) is calculated. Afterward, it is normalized by the standard room-load intensity to derive the load factor so as to extrapolate the AC load required by buildings with different floor areas (Figure 2).

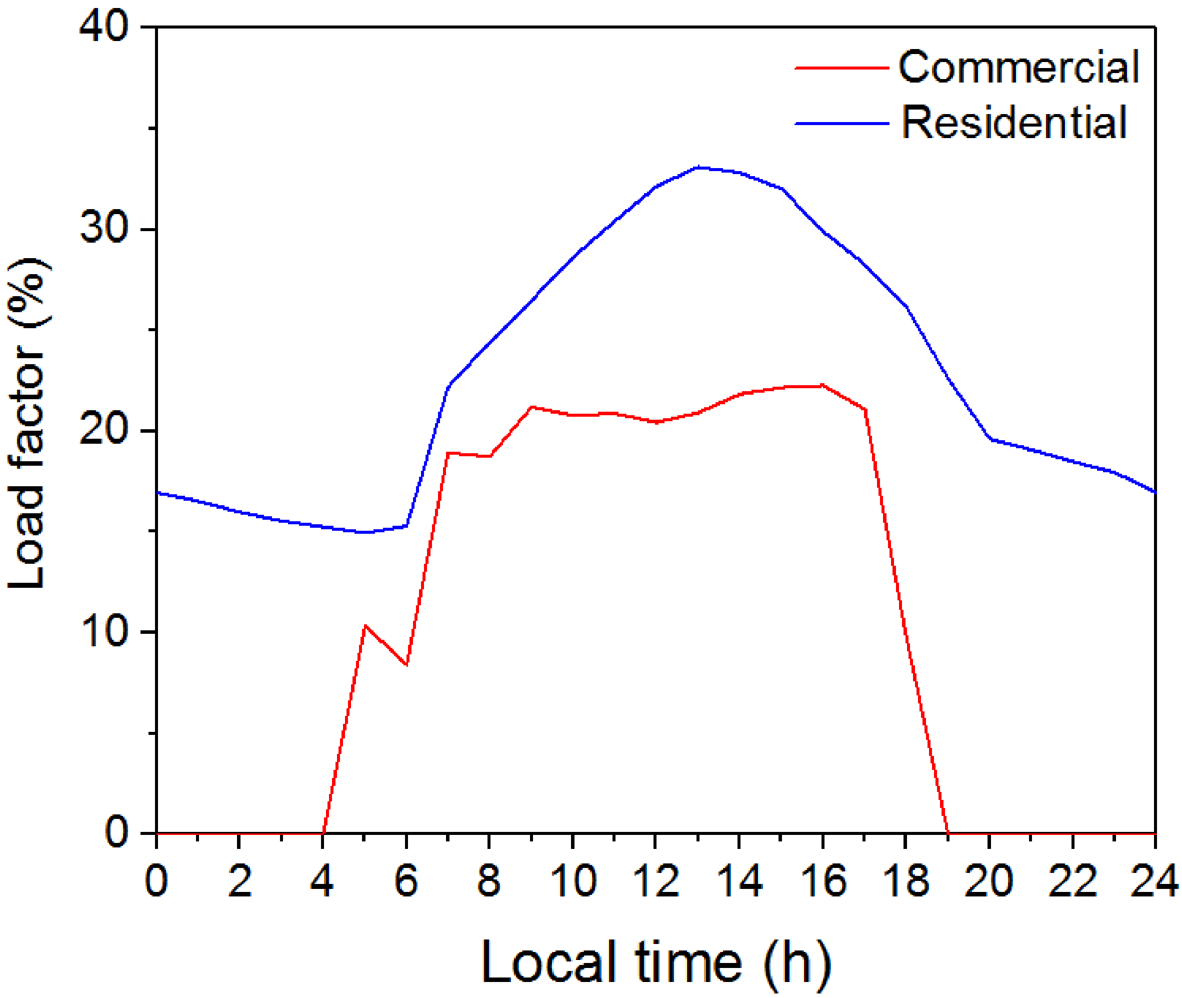

Figure 2. Representative curves of (diurnal) load factor for the commercial and residential buildings in HK.

2.4 Hourly AC Load for Validation

The diurnal AC load during the analysis period can be obtained for each building category i in each model grid P_i by the annual AC electricity consumption (Section 2.2.3) and the representative load curves (Section 2.3; Pappaccogli et al., 2021). The total AC electricity consumption at each model grid for the *i*-th building category ($E_{tot,i}$) is calculated as

$$E_{tot,i} = \overline{E_i} \times A_i = P_i \times \left(24 \times 365 \times \overline{L_i}\right) \quad (1)$$

where $\overline{E_i}$ is the average annual AC electricity consumption for each building category according to EUI, A_i the total floor area of *i*-th building category at each model grid, and $\overline{L_i}$ the daily average of the load consumption curve. P_i obtained from Equation (1) is then multiplied by the annual representative consumption load curves to yield the hourly AC electricity consumption at each model grid.

2.5 Intra-Urban Heterogeneity Analysis

In this study, the UMPs in LCZ classification are further clustered into the following three categories: urban structure, vegetation fraction (VF), and impervious surface thermal properties. Urban structure is a combination of various urban morphology parameters, including SVF, AR, and BSF. There are two reasons to do so: (1) Once the LCZ classification at a model grid is assigned, its SVF, AR, and BSF are determined accordingly (Stewart et al., 2014); (2) Building energy consumption is more accurately described as a function of multiple urban structure indices rather than a single variable (Chen et al., 2020). VF signifies the ratio of greenery to total plan area. The thermal properties of impervious surfaces include heat capacity, thermal conductivity, albedo, and admittance. The aforementioned parameters of each LCZ are summarized in Table 2.

The contribution from individual UMPs to the urban-rural difference in temperature at 2-m height ($\Delta T2$) and AC load (ΔACE) is quantitatively investigated. To calculate $\Delta T2$ and ΔACE, Ta Kwu Ling (TKL) is taken as the rural reference site where has been adopted extensively for urban climate studies (Siu & Hart, 2013). The TKL UMPs (Table 2) are also employed in different scenarios (Section 2.6).

Table 2. Urban morphology parameters (UMPs) for different LCZ types in HK (Wang et al., 2018).

LCZ types	Urban structure			VF[d]	Impervious surface thermal properties		
	SVF[a]	AR[b]	BSF[c]		ISHC[e]	ISTC[f]	ISA[g]
LCZ1	0.25	6	40-70	0.01	1.75	0.77	0.15
LCZ2	0.4	2	40-70	0.05	1.68	0.73	0.15
LCZ3	0.45	1.75	40-70	0.1	1.63	0.69	0.15
LCZ4	0.55	2.75	20-40	0.35	1.54	0.64	0.185
LCZ5	0.60	1.25	20-40	0.3	1.50	0.62	0.185
LCZ6	0.75	1.1	20-40	0.35	1.47	0.60	0.185
LCZ8	0.8	0.2	30-50	0.15	1.80	0.80	0.20
LCZ10	0.75	0.35	20-30	0.45	1.49	0.61	0.16
TKL (reference rural site)	0.8	0.175	10-20	0.3	1.37	0.55	0.185

Remark:

[a] Sky view factor: Ratio of the amount of sky hemisphere visible from ground level to that of an unobstructed hemisphere

[b] Aspect ratio: Mean height-to-width ratio of street canyons (LCZs 1–6) or building spacing (LCZs 8–10)

[c] Building surface fraction: Ratio of building plan area to total plan area (%)

[d] Vegetation fraction: Ratio of vegetation area to total plan area (%)

[e] Impervious surface heat capacity ($\times 10^6$ J m^{-3} K^{-1})

[f] Impervious surface thermal conductivity (J m^{-1} s^{-1} K^{-1})

[g] Impervious surface albedo

To contrast the contribution of individual UMPs among different LCZs and building categories, the relative variation (*RV*) of an analysis variable, such as AC load, is obtained from:

$$RV = \frac{x_{urban} - x_{UMP}}{x_{urban} - x_{rural}} \times 100\% \,. \tag{2}$$

Here, x_{UMP} is the variable extracted from the cases 2 to 4 (Table 5, Section 2.6) in which only one UMP is changed to the same value of the reference rural site (TKL), x_{rural} is the variable extracted from the case 5 in which all the UMPs are the same as those of rural reference site (TKL), x_{urban} is the variable extracted from the real-urban scenario (case 1).

2.6 Model Configuration

The aforementioned LCZs (Section 2.2.1) and building classification maps (Section 2.2.2) are input into the WRF model (ARW version 3.6.1; Brousse et al., 2016). The WRF model is composed of four nested domains with (horizontal) spatial resolution of 9 km (241×181), 3 km (271×181), 1 km (241×181), and 0.33 km (241×181; Figure 3). The LCZBC map over HK of the current WRF is shown in Figure 3. The area ratio and the average distance to coastline (DC) of each LCZBC type are listed in Table 1. To refine the UMPs in the vertical, 51 η levels are used from the ground to 50 hPa in which the (vertical) resolution is as fine as 10 m in the urban canopy. The initial and boundary conditions are obtained from European Centre for Medium-Range Weather Forecasts (ECMWF) ERA-Interim (ECMWF, 2016) with a spatial resolution of 0.75° × 0.75° and a temporal resolution of 6 hours. The time-step increment of this model is 30 seconds and the frequency to write history file is once an hour. Specifically, to study the building energy consumption in summer, the calculation by the WRF model is conducted from June 21 to 28, 2016. The first 40 hours (June 21 to 22, 2016) are the spin-up. Afterward, a 5-day heatwave event (June 23 to 28, 2016) is the archive period for data analysis (Wang et al., 2018).

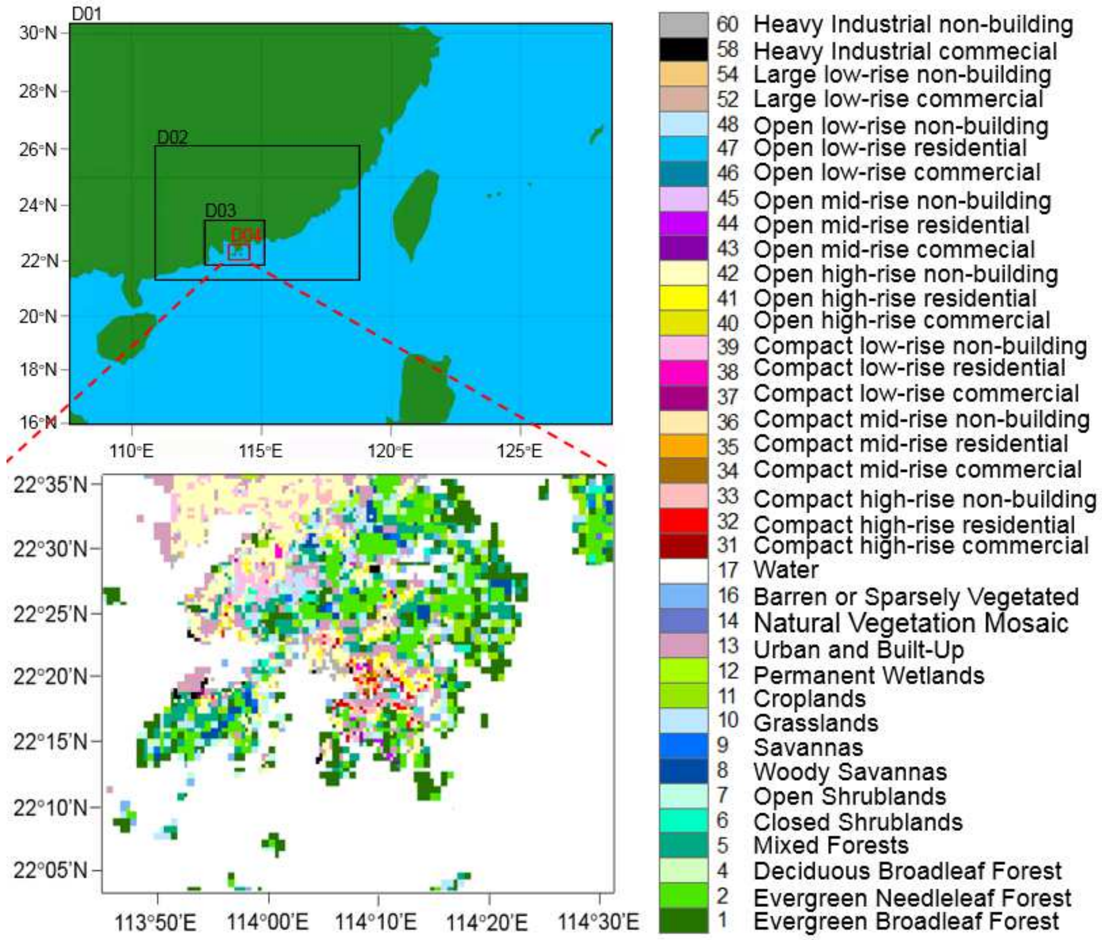

Figure 3. Nested domains in the advanced WRF model, the LULC, and the building category map of HK.

The physical parameterization schemes used in the WRF model are listed in Table 3. To capture urban-scale building energy consumption, the WRF model is coupled with the multi-layer BEP/BEM model. The global landcover data (30 seconds) from Moderate Resolution Imaging Spectroradiometer (MODIS) are used as the default landuse (Friedl et al., 2002). The MODIS urban setting in the innermost domain is replaced by the LCZBC one. LULC is resampled to 333 m resolution based on the dominant class. The modified Fortran WUDAPT-to-WRF (W2W) tool was used to integrate the LCZBC data (Section 2.2) into the WRF model. The general steps are available in the W2W user guide (Martilli et al., 2016) though some interfaces are modified in this study. First, the number of urban classes was extended from 3 to 30 by modifying the BEP/BEM code. The modified BEP/BEM model could also distinguish the characteristics of various LCZBC types such as different cooling fractions. Second, all original Fortran code in the W2W tool package for WUDAPT data (with 10 urban classes) was modified accordingly for the new LCZBC data (with 30 urban classes). Afterwards, the urban parameter lookup table in WRF code was also updated according to different LCZBC types (Table 1). It assigns the corresponding urban morphology and road thermal properties (from WUDAPT data) to each LCZ type in the LCZBC classification, but specific envelope thermophysical properties and AC parameters (Table 4) to building sub-classes (commercial and residential). These building parameters are obtained from government codes, guidelines, surveys, and studies in literature. The building geometries in the non-building areas are replaced by impervious surfaces and no AC system is under operation.

Table 3. Physical parameterization schemes used in the WRF model.

Physics Options	Schemes	References
Boundary Layer	BouLac	(Bougeault & Lacarrere, 1989)
Microphysics	Single-Moment 3-class	(Hong et al., 2004)
Land Surface	Noah	(Chen & Dudhia, 2001)
Cumulus	Kain-Fritsch	(Kain & Fritsch, 1990)
Short Wave Radiation	Dudhia	(Dudhia, 1989)
Long Wave Radiation	Rapid Radiative Transfer Model	(Mlawer et al., 1997)
Surface Urban	BEP/BEM	(Martilli et al., 2002; Salamanca et al., 2010)

Table 4. Parameters of the WRF-BEP/BEM model.

Parameters	Commercial	References	Residential	References
Roof heat capacity (J m^{-3} K^{-1})	1.48×10^{-6}	(Huang & Niu, 2015)	1.46×10^{-6}	(Lin & Deng, 2004)
Roof thermal conductivity (J m^{-1} s^{-1} K^{-1})	0.19	(Huang & Niu, 2015)	0.17	(Lam et al., 2005)
Roof emissivity	0.9	(Ji et al., 2003)	0.9	(Ji et al., 2003)
Roof albedo	0.15	(Ji et al., 2003)	0.15	(Ji et al., 2003)
Wall heat capacity (J m^{-3} K^{-1})	1.56×10^{-6}	(Huang & Niu, 2015)	1.50×10^{-6}	(Lin & Deng, 2004)
Wall thermal conductivity (J m^{-1} s^{-1} K^{-1})	0.77	(Huang & Niu, 2015)	0.69	(Yu et al., 2020)
Wall emissivity	0.9	(Ji et al., 2003)	0.9	(Ji et al., 2003)
Wall albedo	0.15	(Ji et al., 2003)	0.15	(Ji et al., 2003)
Peaked heat generation by equipment (W m^{-2})	35	(Ma & Yu, 2020)	21.5	(Lam et al., 2005)
AC coefficient of performance (COP)	3.2	(Chan, 2011)	2.6	(HKEMSD, 2015)
Peaked number of occupants per unit floor area (person m^{-2})	0.088	(Huang & Niu, 2015)	0.08	(Yu et al., 2020)
Internal set-point temperature (°C)	25	(Huang & Niu, 2015)	25	(Yu et al., 2020)
Internal set-point specific humidity (kg kg^{-1})	0.0086	(Huang et al., 2021)	0.0086	(Huang et al., 2021)

To acquire more accurate AC load in HK, three parameters are introduced to the BEP/BEM model: (1) building vacancy ratio *a* (9% and 3.8% for commercial and residential buildings, respectively; HK.Government, 2016); (2) the ratio of AC floor area to total floor area *b* (90.25% and 64% for commercial and residential buildings, respectively; Xu et al., 2018); and (3) AC usage ratio *c* (1 during heatwave event). The BEP/BEM configuration was modified to introduce the cooling faction for the corresponding LULC types. Hence, the actual electricity load (E_C^{P-AC}) is calculated as follows

$$E_C^{P-AC} = E_c \times (1-a) \times b \times c. \quad (3)$$

In this study, the impacts of urban structure, vegetation fraction, and impervious surface thermal properties on UHII and building energy consumption are compared. To test the sensitivity of urban-rural climate and energy discrepancy to UMPs, five sets of numerical experiment, including one real scenario (URBAN-LCZBC) and four hypothetical scenarios with modified UMPs, are carried out (Table 5). The four hypothetical scenarios are: (1) a low-density, low-rise building scenario (RURAL-STRUCTURE) by changing the building/street structure parameters of all urban areas to those of the reference rural site (TKL); (2) a green scenario (RURAL-GREEN) by changing the vegetation fraction of all city areas to that of the reference rural site (TKL); (3) a scenario (RURAL- IMPERVIOUS-SURFACE) by changing the thermal properties of impervious surfaces of all built areas to those of the reference rural site (TKL); and (4) an all-rural scenario (ALLRURAL) by changing the UMPs of all built areas to those of the reference rural site (TKL). These UMPs were set by modifying the urban parameter lookup table in WRF configuration.

Table 5. Design of numerical experiments.

Scenario		Numerical experiments	Model setup
Real	1	URBAN-LCZBC	WRF coupled to BEP/BEM with combination of LCZ data and building category data (LCZBC) as the landuse configuration
Hypothetical	2	RURAL-STRUCTURE	Same as URBAN-LCZBC but the building/street structure parameters of all urban areas are changed to those of the rural reference site (TKL)
	3	RURAL-GREEN	Same as URBAN-LCZBC but the vegetation fraction of all urban areas is changed to that of the rural reference site (TKL)
	4	RURAL-IMPERVIOUS-SURFACE	Same as URBAN-LCZBC but the thermal properties of impervious surfaces in all urban areas are changed to those of rural reference site (TKL)
	5	ALLRURAL	Same as URBAN-LCZBC but the urban morphology parameters (UMPs) of all urban areas are changed to those of rural reference site (TKL)

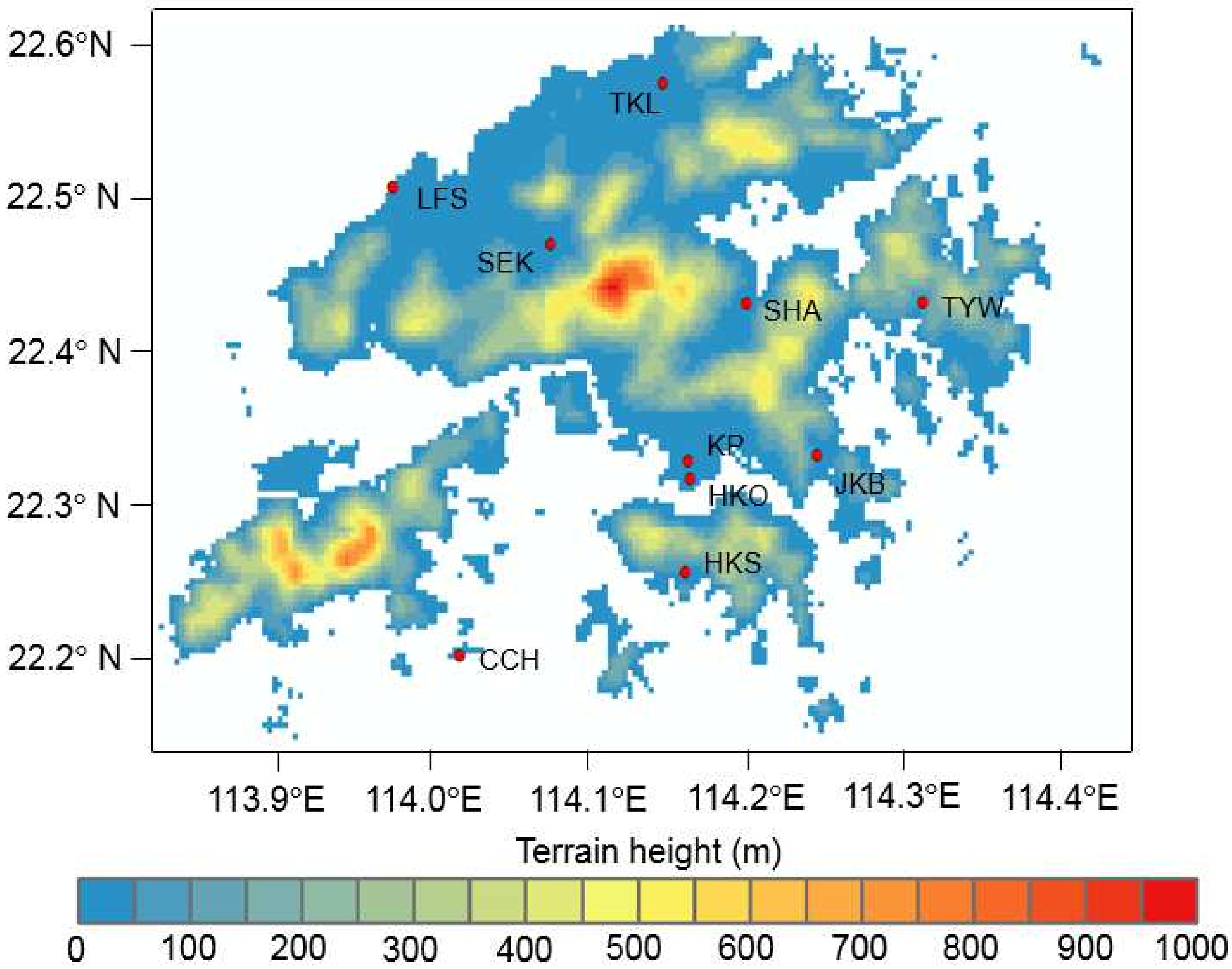

Figure 4. Location of the (10 nos.) weather stations in HK.

Table 6. Root-mean-square errors (RMSEs) between the predicted and observed 2-m temperature (*T*2), 2-m RH (*RH*2), and 10-m wind speed (*W*10) at the 10 weather stations operated by HKO (HKO, 2022).

Station	Classification	LCZ type	RMSEs		
			*T*2 (°C)	*RH*2 (%)	*W*10 (m/s)
HKO	urban	LCZ1	1.41	9.65	1.46
KP	urban	LCZ4	0.86	8.44	1.14
HKS	suburban	LCZ5	1.11	8.79	1.21
JKB	suburban	LCZ4	1.57	9.80	0.72
LFS	suburban	LCZ4	0.98	8.48	1.36
SEK	suburban	LCZC	1.25	8.99	1.53
SHA	suburban	LCZ6	1.14	7.09	0.91
CCH	rural	LCZA	1.25	7.69	1.16
TKL	rural	LCZ6	1.31	8.87	0.88
TYW	rural	LCZ4	1.61	8.41	/

3. Model Validation

3.1 Meteorological Variables

The current WRF-LCZBC modeling results are validated by the observation from a network of 10 weather stations operated by the HK Observatory (HKO; Figure 4). The root-mean-square errors (RMSEs) are used as the metrics, evaluating the model performance in terms of: (1) 2-m temperature (*T*2); (2) 2-m RH (*RH*2); and (3) 10-m wind speed (*W*10). As shown in Table 6, all the RMSEs are within acceptable ranges (Hwang et al., 2019), supporting the reliability of the current WRF-LCZBC model. In particular, the RMSEs of *T*2 at urban stations (0.86-1.41 °C) are quite uniform that are compatible to those at suburban (0.98-1.57 °C) and rural (1.31-1.61 °C) stations. The average RMSEs of 2-m RH at suburban (*RH*2 = 8.72%) and rural (*RH*2 = 7.55%) stations are lower than those at urban stations (*RH*2 = 9.05%). The calculation of 10-m wind speeds at all the stations is acceptable as well according to the benchmark of US EPA (RMSEs of *W*10 < 2 m/s; US.EPA, 2007).

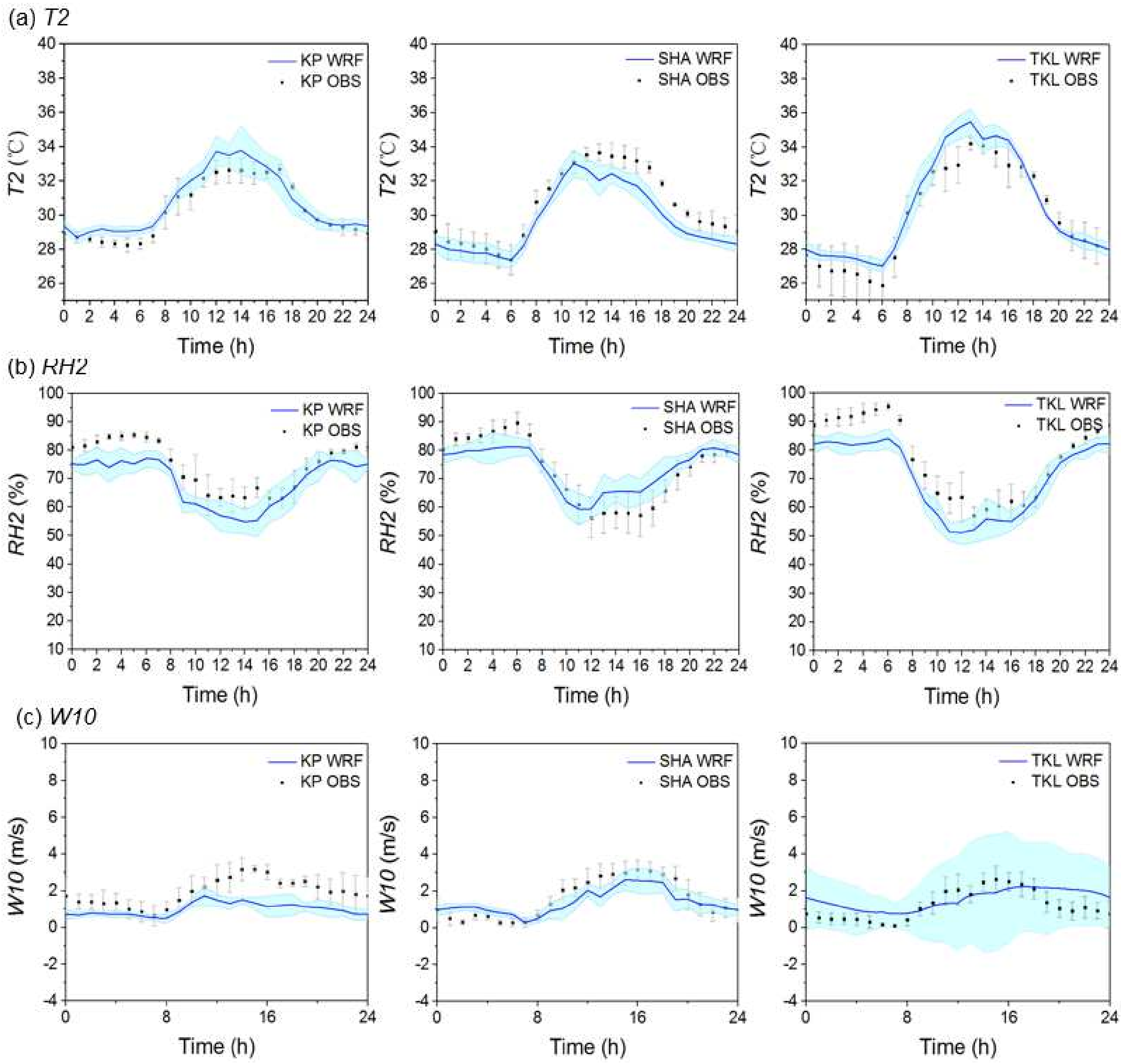

Figure 5. Comparison between WRF and observed results for average diurnal cycle ±1 standard deviation of (a) 2-m temperature (*T*2), (b) 2-m relative humidity (*RH*2), and (c) 10-m wind speed (*W*10) at KP, SHA, and TKL sites.

To further evaluate the model functionality, we compare the diurnal profiles of *T*2, *RH*2, and *W*10 between the WRF results and the field measurements (Figure 5) at KP (urban), SHA (suburban), and TKL (rural). Their temporal variations agree well at all sites though mild discrepancies in the extreme values are observed. A negative bias is noted at both urban and suburban stations that indicates a gentle underprediction of the peaked *W*10. It could be caused by the model interpolation from the first vertical level to 10 m above ground level (Mughal et al., 2019). Besides, the selection of PBL scheme would cause different bias, which needs certainly further investigation. The peaked *RH*2 at urban and suburban areas are underpredicted. It is mainly attributed to the (over) simplification of assuming all urban vegetation tiles as grassland. The peaked 2-m temperatures are overpredicted and underpredicted, respectively, at urban and suburban weather stations. It could be attributed to the discrepancy between the WRF spatial resolution (333 m) and the LCZ data resolution (100 m) in the innermost Domain 4 and the subsequent model interpolation using only the dominant LCZ type at one grid point. For instance, an urban weather station is characterized at a model grid (333×333 m^2) as the open high-rise region (LCZ4) due to the majority urban classes. Whereas, it is actually located in sparsely constructed areas (LCZ9-C/R).

Table 7. Root-mean-square errors (RMSEs) of AC load between the WRF and observed results for each LCZBC category.

LCZ	RMSE (W/m^2)	
	Commercial	Residential
LCZ1	15.659	8.607
LCZ2	13.575	3.237
LCZ3	8.991	2.640
LCZ4	9.176	2.031
LCZ5	7.913	1.568
LCZ10	4.094	2.648

3.2 Energy Consumption

The WRF-LCZBC-calculated AC load for each LCZBC in HK compares well with the observed one (Table 7) in which the RMSEs are within acceptable range (Takane et al., 2017). The observed diurnal curves of AC load are obtained from the spatial average of EUI data (Section 2.4). It is noteworthy that the RMSEs for commercial-dominant areas (9.90%) of all LCZs are larger than those for residential-dominant areas (3.46%) by almost threefold. The different RMSEs are attributed to the different energy consumption in commercial and residential areas. Their nominal values are about the same.

Generally, WRF describes reasonably well the diurnal behaviors of AC load for all the LCZBC categories compared to the observed ones (Figure 6). The peaked AC load is slightly overestimated for almost all the LCZBC categories except LCZ10-C and LCZ10-R. The reason could be the dissimilar spatial resolution between WRF and LCZBC described previously in Section 3.1. Besides, the nighttime AC load for both commercial and residential areas is slightly overestimated for almost all the LCZs. It could be attributed to the insufficient AC categories being considered in this WRF model. In the HK context, the direct cooling system (DCS; using seawater for cooling) or evaporative air conditioners (EAC) are installed in some large office buildings and a small portion of contemporary residential buildings. These AC systems could lower outdoor air temperature because latent (instead of sensible) heat contributes most to AC exhaust removal (Wang et al., 2018). By reducing ambient temperature, DCS and EAC have been reported to reduce energy consumption compared with dry air conditioners which emit almost fully in sensible heat (Xu et al., 2018). Some studies included EAC in BEM to improve the simulation of urban-scale AC load (Ortiz et al., 2022). DCS is worthy to be considered based on enhanced urban canopy and BEM.

Furthermore, the WRF-calculated AC load is more sensitive to the outdoor condition in diurnal cycle than its observation counterpart. It could be attributed to the scanty details in some building thermal parameters (such as roof and wall conductivity) or AC system settings (such as set-point temperature). In reality, there exist diversified building characteristics or AC settings even for the same building types (commercial or residential). Ortiz et al. (2022) found that building energy burden during summer is sensitive to rooftop albedo and AC target temperature. They also reported the WRF-calculated AC load is less sensitive to time-of-day than its observation counterpart because of the scanty details in the urban-parameter lookup table. The current WRF model assumed consistent and static parameters of a building type that might overestimate the heat fluxes into buildings or the set-point temperature. Eventually, the WRF-calculated AC load is highly sensitive to the outdoor conditions.

Besides, the current WRF model (with 30 LCZBC urban classes) has been evaluated against the standard WRF model (with 3 urban classes) and the WRF-WUDAPT model (with 10 LCZ urban classes) in our previous work (Du et al., 2023). The refined LULC configuration enables this WRF model to represent more comprehensively the meteorological variables and AC load.

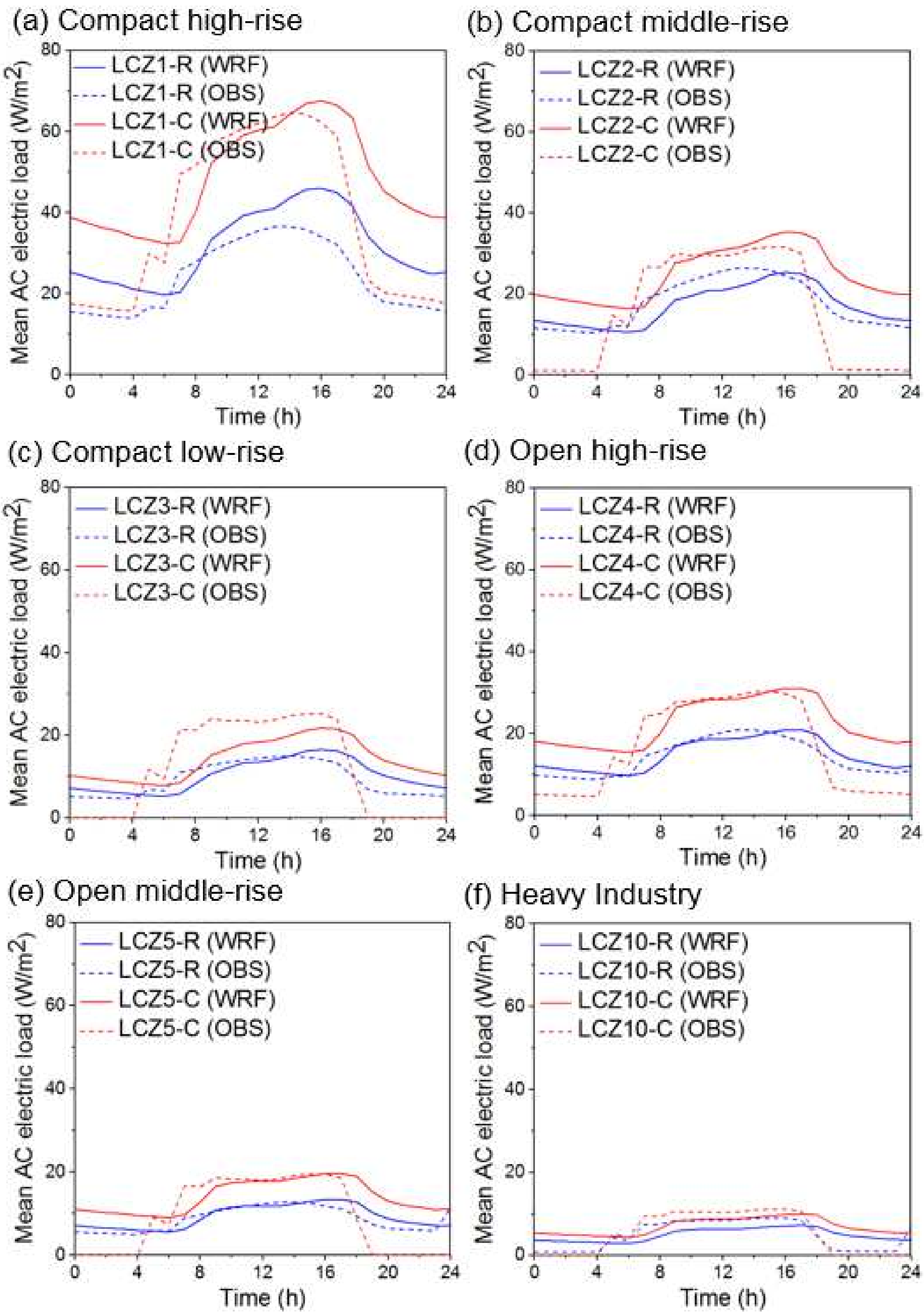

Figure 6. Comparison between WRF and observed results for average diurnal cycle of AC load for different LCZs and building categories.

4. Results and Discussion

To quantify the UHII, the differences in 2-m temperature ($\Delta T2_{urban\text{-}rural}$), sensible cooling demand ($\Delta SCD_{urban\text{-}rural}$), and AC load ($\Delta ACE_{urban\text{-}rural}$) between the real-urban (URBAN-LCZBC) and all-rural (ALLRURAL) scenarios are compared. Positive $\Delta T2_{urban\text{-}rural}$ signifies UHI, otherwise urban cool island. In this section, we present the spatio-temporal variation of UHIIs ($\Delta T2_{ump}$), sensible cooling demand (ΔSCD_{ump}), and building energy consumption (ΔACE_{ump}) induced by specific UMPs. Furthermore, the sensitivity of urban climate and AC load to urban structure, vegetation fraction, and impervious surfaces is conducted for different LCZBCs.

4.1 Temperature distribution

In this section, the relationship between LCZBC types and spatial distribution of 2-m temperature (***T***2) is analyzed. For brevity, only the results for the two peaks at daytime (1400 LST) and nighttime (2100 LST) are shown in Figure 7. The high temperature is concentrated in compact or high-rise urban areas for both daytime (29.97-40.99 °C) and nighttime (25.41-33.76 °C, Figures 7a and b), with a pattern similar to that of urban landscape classification (Figure 1). It signifies that the various urban morphology and building thermal properties of different urban land use types are important factors to the spatial heterogeneity of air temperature. Figures 7b and c show the ***T***2 variation in each landscape type (LCZBC). The average ***T***2 among different LCZBCs has the largest differences of 3.96 °C and 2.85 °C in daytime and at nighttime, respectively. The compact building areas (LCZ 1, 2, and 3) have 2.22 °C (1.32 °C) higher temperature than open building areas (LCZ 4, 5 and 6) in daytime (at nighttime). Besides, the average ***T***2 is around 0.4 °C (0.5 °C) hotter in high-rise building areas (LCZ1 and LCZ4) than their midrise/low-rise counterparts (LCZ 2, 3, 5 and 6) in daytime (at nighttime). The high-density and high-rise building areas (LCZ 1 to 4) are hotter than others. It could be attributed to the high aspect ratio (1.75 ≤ AR ≤ 6) in these areas, reinforcing heat trap and weakening heat dissipation.

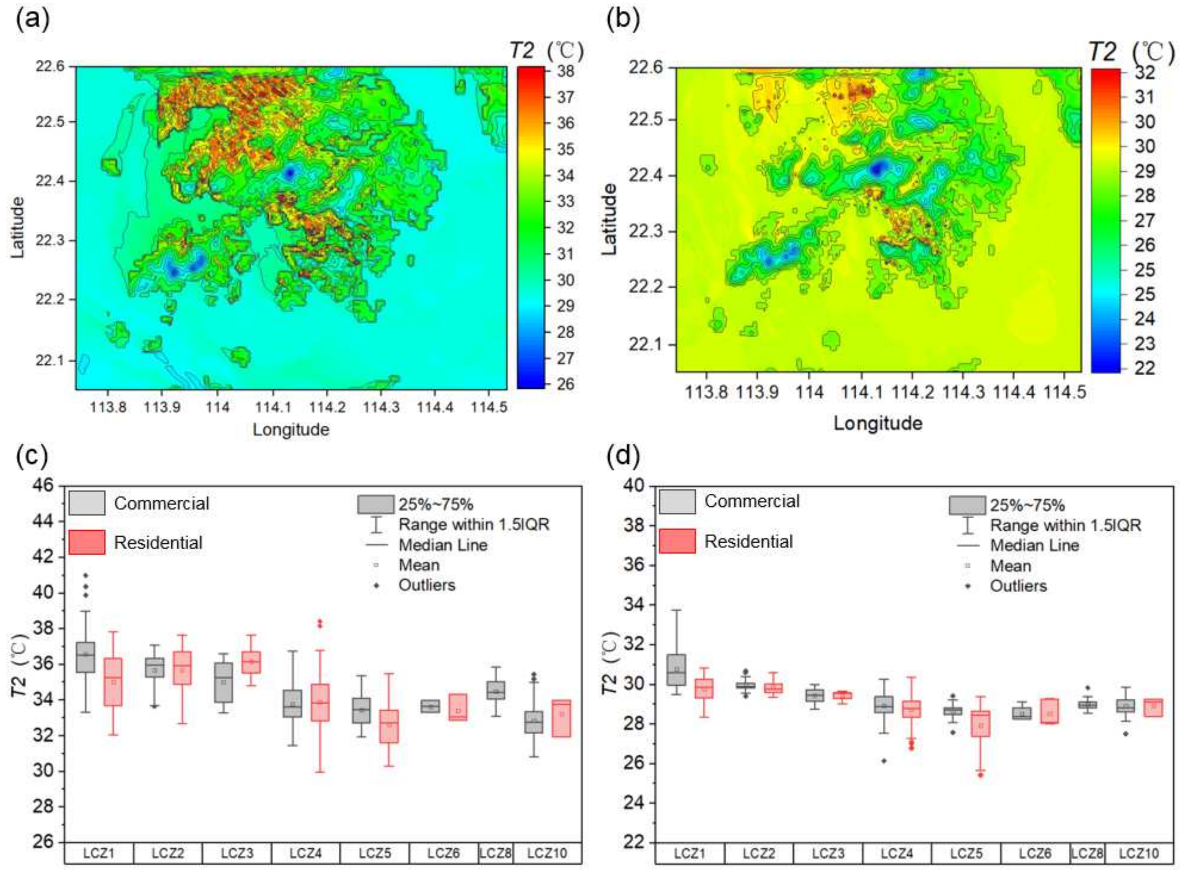

Figure 7. 2-m air temperature *T*2 (°C) distribution over Hong Kong at (a) 1400 LST and (b) 2100 LST; and 2-m air temperature *T*2 (°C) variation of each landscape type at (c) 1400 LST and (d) 2100 LST.

For most LCZs, the commercial-dominant areas are warmer than residential-dominant areas. The largest difference (1.56 ºC) between them occurs in compact high-rise building areas (LCZ1). Based on the refined building characteristics, the present model captured the spatially inhomogeneous anthropogenic heat (AH). As such, the AH heterogeneity in commercial- (higher AH) and residential-dominant (lower AH) areas was well represented. Moreover, the deeper street canyons with higher AR in LCZ1 aggravated the anthropogenic heat trap in commercial-dominant areas.

4.2 Impact of Urban Structure

The UHIIs ($\Delta T2_{structure}$) attributed to urban structure are measured by the differences between the real scenario (URBAN-LCZBC) and scenario 2 (RURAL-STRUCTURE) cases. To quantify the urban structure contribution to real-urban-rural-climate discrepancy, the relative UHII variations ($\Delta T2_{structure}/\Delta T2_{urban\text{-}rural}$) are also calculated by Equation (2). Figure 8 compares the diurnal variation of the ensemble averaged $\Delta T2_{structure}$ and $\Delta T2_{structure}/\Delta T2_{urban\text{-}rural}$ for the LCZBCs in HK. Here, ensemble average is the hourly averaged property of a LCZBC. Urban structure tends to induce notable UHI at nighttime but insignificant or even urban cool island in daytime. Here, the nighttime and daytime are defined from 1801 to 0759 LST and from 0800 to 1800 LST, respectively. The spatial average of maximum $\Delta T2_{structure}$ (= 0.59 °C) is observed at 0600 LST when the urban structure apparently contributes most to UHII ($\Delta T2_{structure}/\Delta T2_{urban\text{-}rural}$ = 40.33%). Here, spatial average is the hourly average at each model grid. Compared with the rural built structure, the urban structure possesses a lower SVF and a higher AR. A lower SVF implies less exposure to the sky that ends up with less incoming solar radiation (daytime heat gain) or outgoing longwave radiation (nighttime heat loss). On the other hand, deeper street canyons have higher ARs where the heat dissipation is weakened (Yu et al., 2020). As such, the low-SVF, high-AR urban structure gains less heat in daytime (lower $\Delta T2_{structure}$) and dissipates less heat at nighttime (higher $\Delta T2_{structure}$). Moreover, urban structure is more massive than its rural counterpart that captures more solar heat in daytime (cooler air temperature) but releases more heat at nighttime (hotter air temperature).

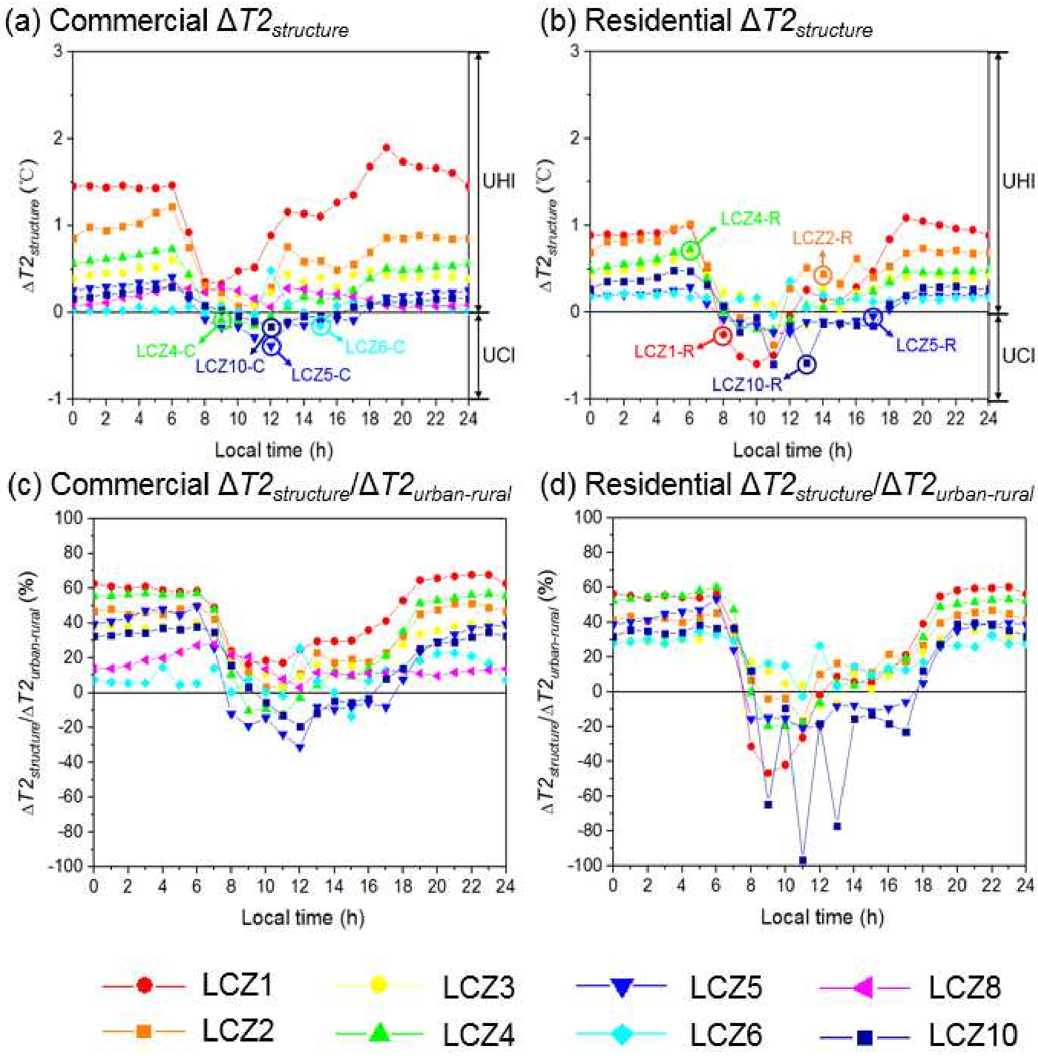

Figure 8. Diurnal variation of ensemble-averaged UHIIs ($\Delta T2_{structure}$) induced by urban structure of (a) commercial-dominant and (b) residential-dominant areas together with ensemble-averaged relative variation of UHIIs ($\Delta T2_{structure}/\Delta T2_{urban\text{-}rural}$) induced by urban structure of (c) commercial-dominant and (d) residential-dominant areas for different LCZBCs.

The daytime urban cool island (-0.60 ~ -0.01 °C) for compact residential (LCZ1 to 3-R), open (LCZ4 to 6-C/R), and industrial (LCZ10-C/R) areas could be explained by the low SVF and the massive volume of urban structures. The negatively correlated $\Delta T2_{structure}$ is consistent with previous studies (Chen et al., 2012; Yu et al., 2020). It is noteworthy that urban cool island would occur more often in residential-dominant areas in daytime than their commercial-dominant counterparts. Although low SVF and the massive volume enable urban structures to be cooler than those in rural areas (UCI) with the same solar radiation, anthropogenic heat exhaust from commercial AC (as another heat source) is higher than residential AC. Hence, the UCI is modest in commercial areas in daytime.

Energy impact in response to urban structure is further tested by the difference in sensible cooling demand ($\Delta SCD_{structure}$) between the cases UBRAN-LCZBC and RURAL-STRUCTURE. For most LCZBCs, urban structure induces significantly $\Delta SCD_{structure}$ in daytime but not at nighttime (Figures 9 a and b). Whereas, $\Delta SCD_{structure}$ is rather uniform in the diurnal cycle for open low-rise (LCZ6-C/R) and large low-rise commercial (LCZ8-C) areas. The spatial average of $\Delta SCD_{structure}$ (= 18.69 w/m^2) is peaked at 1600 LST. The diurnal variation of $\Delta SCD_{structure}$ is inconsistent with that of $\Delta T2_{structure}$ and $\Delta T2_{structure}/\Delta T2_{urban\text{-}rural}$. Therefore, urban structure induces substantial $\Delta SCD_{structure}$ but not $\Delta T2_{structure}$ in daytime. It is in turn implied that urban structure influences building energy consumption not only by modifying outdoor temperatures indirectly but also by building physics directly.

To quantify the contribution from urban structure to real urban-rural energy discrepancy, the relative variations of additional SCD ($\Delta SCD_{structure}/\Delta SCD_{urban\text{-}rural}$) are also calculated by Equation (2). Figures 9 c and d compare the diurnal variation of the ensemble-averaged $\Delta SCD_{structure}/\Delta SCD_{urban\text{-}rural}$ for commercial- and residential-dominant LCZBCs, respectively. Analogous to $\Delta T2_{structure}/\Delta T2_{urban\text{-}rural}$, it is found that $\Delta SCD_{structure}/\Delta SCD_{urban\text{-}rural}$ is elevated at nighttime than that in daytime. The spatial average of $\Delta SCD_{structure}/\Delta SCD_{urban\text{-}rural}$ (34.52%) is peaked at 0600 LST, hence, urban structure plays a more prominent role in building energy consumption at nighttime than does in daytime. Unlike $\Delta T2_{structure}/\Delta T2_{urban\text{-}rural}$, $\Delta SCD_{structure}/\Delta SCD_{urban\text{-}rural}$ exhibits a rather uniform diurnal variation that is caused by the time lag between outdoor temperature and building energy consumption.

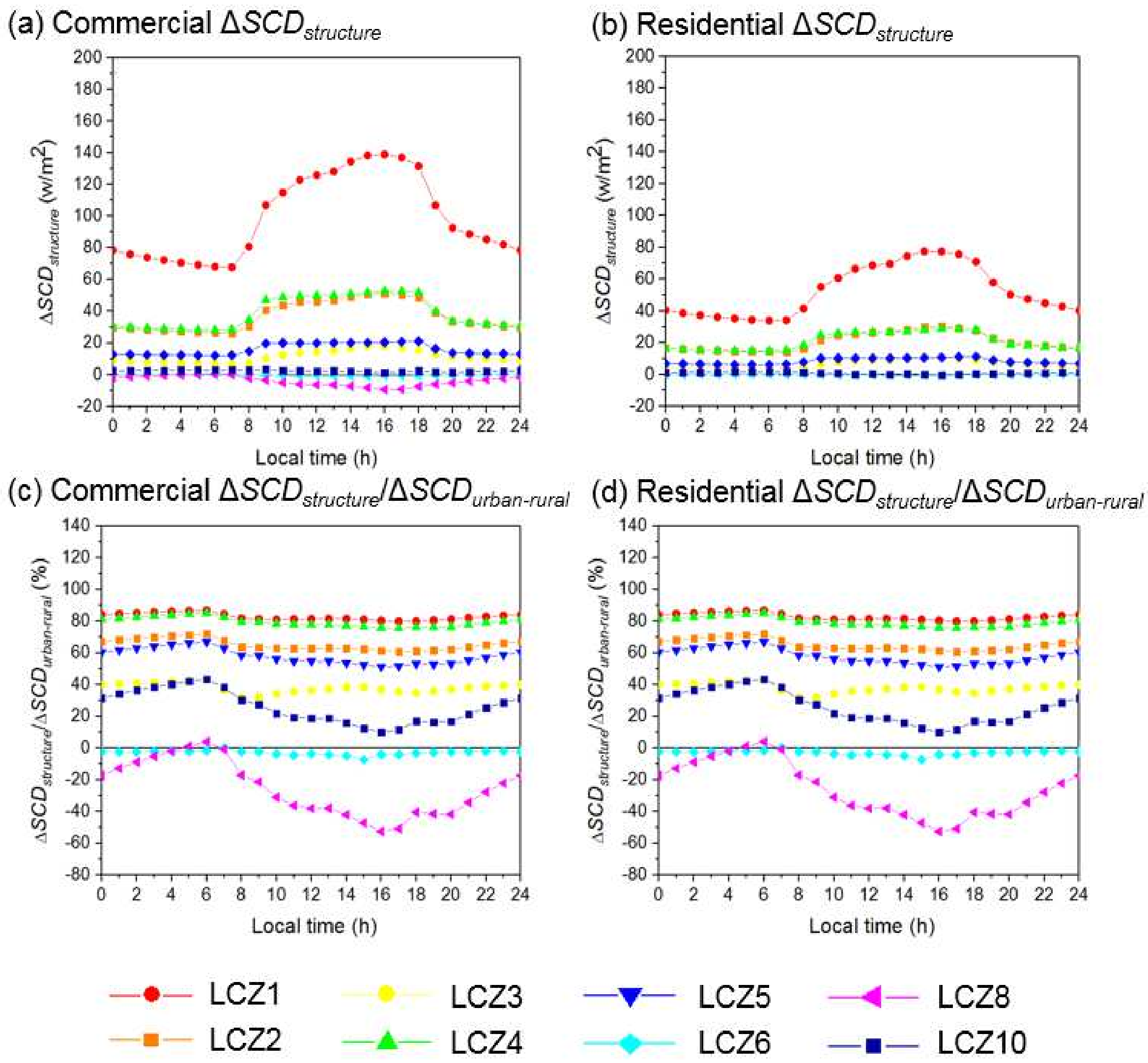

Figure 9. Diurnal variation of ensemble-averaged sensible cooling demand ($\Delta SCD_{structure}$) induced by urban structure of (a) commercial-dominant and (b) residential-dominant areas together with ensemble-averaged relative variation of sensible cooling demand ($\Delta SCD_{structure}/\Delta SCD_{urban\text{-}rural}$) induced by urban structure of (c) commercial-dominant and (d) residential-dominant areas for different LCZBCs.

The variations of $\Delta T2_{structure}/\Delta T2_{urban\text{-}rural}$ and $\Delta ACE_{structure}/\Delta ACE_{urban\text{-}rural}$ closely follow the ARs of LCZBCs (Figure 10) that demonstrate the importance of urban structure and configuration to building energy consumption. Apparently, urban structure plays a key role in UHII and AC load for compact high-rise (LCZ1) and open high-rise (LCZ4) areas where ARs are relatively high ($2.75 \leq AR \leq 6$). Unlike other LCZs, average $\Delta ACE_{structure}/\Delta ACE_{urban\text{-}rural}$ is negative in open low-rise (LCZ6-C/R) and large low-rise (LCZ8-C) areas. The negative $\Delta ACE_{structure}/\Delta ACE_{urban\text{-}rural}$ in LCZ6-C/R is due to the aforementioned negative $\Delta T2_{structure}$ caused by the low SVF (Figure 8). The decrease in urban-structure-induced AC load in LCZ8-C could be attributed to the more massive building volume which is able to store more heat. Hence, the indoor temperatures in urban dwellings are less sensitive to the outdoor extremities than their rural counterparts. In addition, for all the LCZs, the urban structure induces larger $\Delta T2_{structure}/\Delta T2_{urban\text{-}rural}$ (= 23.15%) and $\Delta ACE_{structure}/\Delta ACE_{urban\text{-}rural}$ (= 50.93%) in commercial-dominant areas than does residential-dominant areas ($\Delta T2_{structure}/\Delta T2_{urban\text{-}rural}$ = 18.62% and $\Delta ACE_{structure}/\Delta ACE_{urban\text{-}rural}$ = 48.77%). This difference is attributed to the heavier AC load in commercial-dominant areas, exhausting more anthropogenic heat than that in residential-dominant areas. The additional exhaust reinforces the heat trap in urban areas that results in higher $\Delta T2_{structure}$ and more vigorous energy feedback $\Delta ACE_{structure}$.

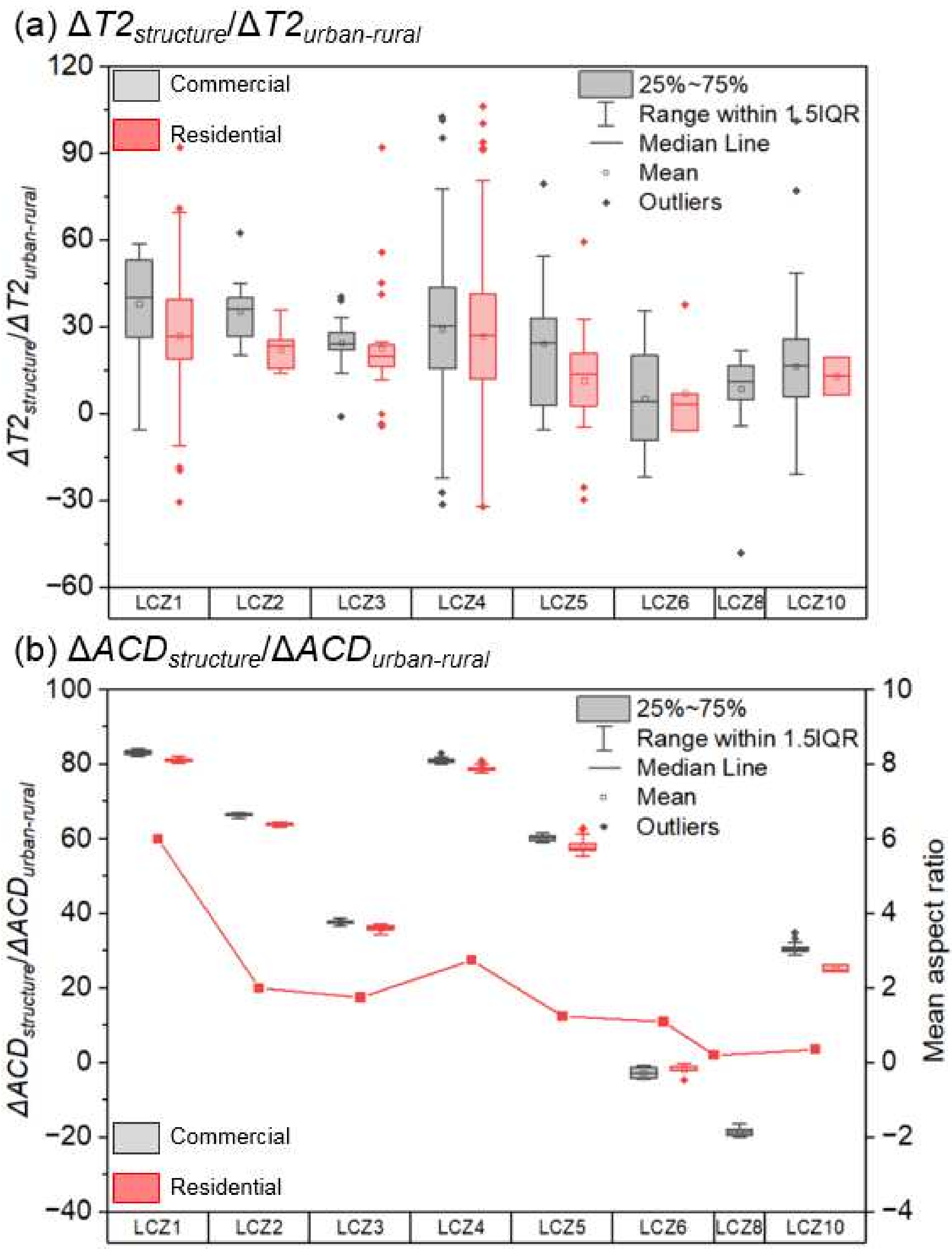

Figure 10. Relative variations of (a) UHIIs ($\Delta T2_{structure}/\Delta T2_{urban\text{-}rural}$) together with (b) air-conditioning load ($\Delta ACE_{structure}/\Delta ACE_{urban\text{-}rural}$) and the ARs (solid lines) plotted as functions of LCZs.

4.3 Impact of Vegetation Fraction

To investigate the impact of urban-rural vegetation fraction difference (ΔVF) on urban climate, the ΔVF-induced UHII ($\Delta T2_{vf}$) is compared with the difference in temperatures between real scenario (URBAN-LCZBC) and scenario 3 (RURAL-GREEN) cases. Besides, the relative UHII variations ($\Delta T2_{vf}/\Delta T2_{urban-rural}$) is calculated by Equation (2) to quantify how ΔVF contributes to the discrepancy between real-urban and real-rural climate. Figure 11 shows the diurnal variations of the ensemble-averaged $\Delta T2_{vf}$ and $\Delta T2_{vf}/\Delta T2_{urban-rural}$ for each LCZBC in HK. UHI is induced by ΔVF all-day-long in which the impact is more notable in daytime. The spatial averages of maximum $\Delta T2_{vf}$ (2.10 °C) and $\Delta T2_{vf}/\Delta T2_{urban-rural}$ (106.26%) occur at 1300 and 1000 LST, respectively. The elevated temperatures in the URBAN-LCZBC case could partly be attributed to the configuration of the sensitivity tests. The natural vegetation in urban areas is replaced by low-albedo, artificial surfaces. Subsequently, three drawbacks: (1) weakened evapotranspiration processes with increased sensible heat and reduced latent heat (Arghavani et al., 2020), (2) low specific heat capacity, resulting in hotter temperatures at the same amount of incoming solar radiation, and (3) low albedo with more heat gain.

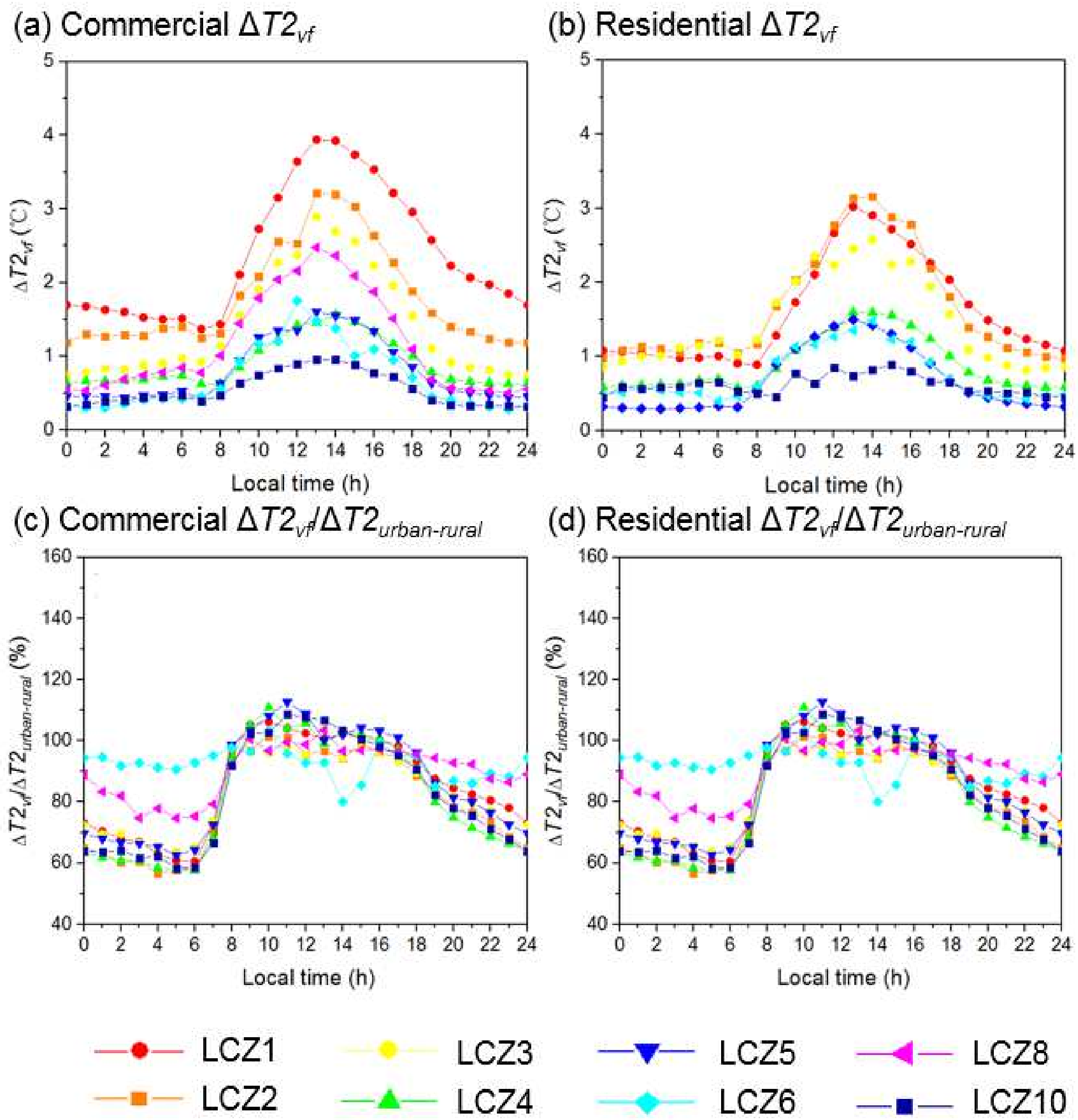

Figure 11. Diurnal variation of ensemble-averaged UHII ($\Delta T2_{vf}$) induced by urban-rural vegetation fraction difference (ΔVF) of (a) commercial-dominant and (b) residential-dominant areas together with ensemble-averaged relative variation of UHIIs ($\Delta T2_{vf}/\Delta T2_{urban\text{-}rural}$) induced by ΔVF of (c) commercial-dominant and (d) residential-dominant areas for different LCZBCs.

The ΔVF-induced sensible cooling demand (ΔSCD_{vf}) is calculated by the difference between the cases UBRAN-LCZBC and RURAL-GREEN to contrast the associated building energy consumption. ΔVF arouses ΔSCD_{vf} in daytime but not at nighttime (Figures 12 a and b). The spatial average of maximum ΔSCD_{vf} (25.54 w/m^2) appears at 1600 LST. Different from urban structure, the diurnal variation of ΔSCD_{vf} is consistent with its $\Delta T2_{vf}$ and $\Delta T2_{vf}/\Delta T2_{urban\text{-}rural}$ counterparts. One of the reasons is that vegetation surface only indirectly influences building energy consumption via outdoor temperatures but not directly building thermal processes. Moreover, to assess ΔVF contribution to the difference in real urban-rural building energy consumption, the relative variation of additional SCD ($\Delta SCD_{vf}/\Delta SCD_{urban\text{-}rural}$) is calculated by Equation (2). Figures 12 c and d display the diurnal variation of the ensemble averaged $\Delta SCD_{vf}/\Delta SCD_{urban\text{-}rural}$ for the LCZBCs in HK. $\Delta T2_{vf}$ (2.10 °C) is peaked at 1300 LST that occurs 3 hours earlier than its $\Delta SCD_{vf}/\Delta SCD_{urban\text{-}rural}$ counterpart (56.69% at 1600 LST). The time lag demonstrates the delayed response of building energy consumption to outdoor temperatures.

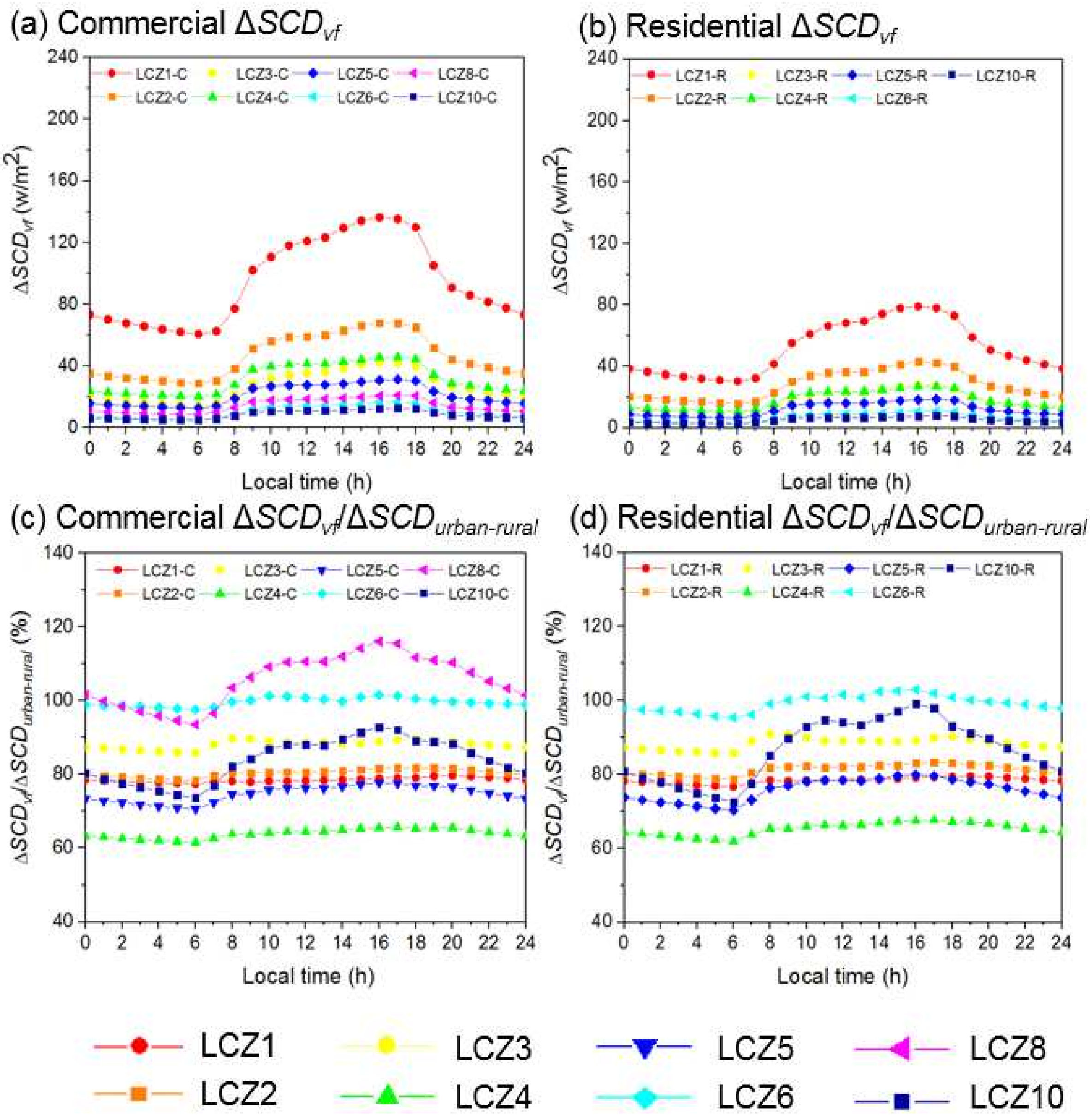

Figure 12. Diurnal variation of ensemble-averaged sensible cooling demand (ΔSCD_{vf}) induced by urban-rural vegetation fraction difference (ΔVF) of (a) commercial-dominant and (b) residential-dominant areas together with ensemble-averaged relative variation of sensible cooling demand ($\Delta SCD_{vf}/\Delta SCD_{urban\text{-}rural}$) induced by ΔVF of (c) commercial-dominant and (d) residential-dominant areas for different LCZBCs.

The variation of $\Delta T2_{vf}/\Delta T2_{urban\text{-}rural}$ and $\Delta ACE_{vf}/\Delta ACE_{urban\text{-}rural}$ is calculated to compare the influence of ΔVF among different LCZBCs (Figure 13). Greenery reduces UHII and building energy consumption in all the LCZBCs. $\Delta T2_{vf}/\Delta T2_{urban\text{-}rural}$ and $\Delta ACE_{vf}/\Delta ACE_{urban\text{-}rural}$ do not simply follow the mean unnatural area fraction. ΔVF plays a more important role in compact/open mid-rise (LCZ2/LCZ5) and low-rise (LCZ3/6) areas. It is because greenery substantially modifies surface temperatures that in turn influences building energy consumption. In particular, most of the buildings in these two areas are within the effective height from vegetation (about 0 to 10 m). Other than compact high-rise areas (LCZ1), the daily average of $\Delta ACE_{vf}/\Delta ACE_{urban\text{-}rural}$ in residential-dominant areas (81.73%) is comparable that in commercial-dominant areas (81.05%) in all the LCZs (Figure 13). It is because ΔVF affects outdoor temperatures then subsequently the building energy consumption. The cooling demand of residential buildings is more sensitive to the ambient temperatures (Toparlar et al., 2018; Yang et al., 2020).

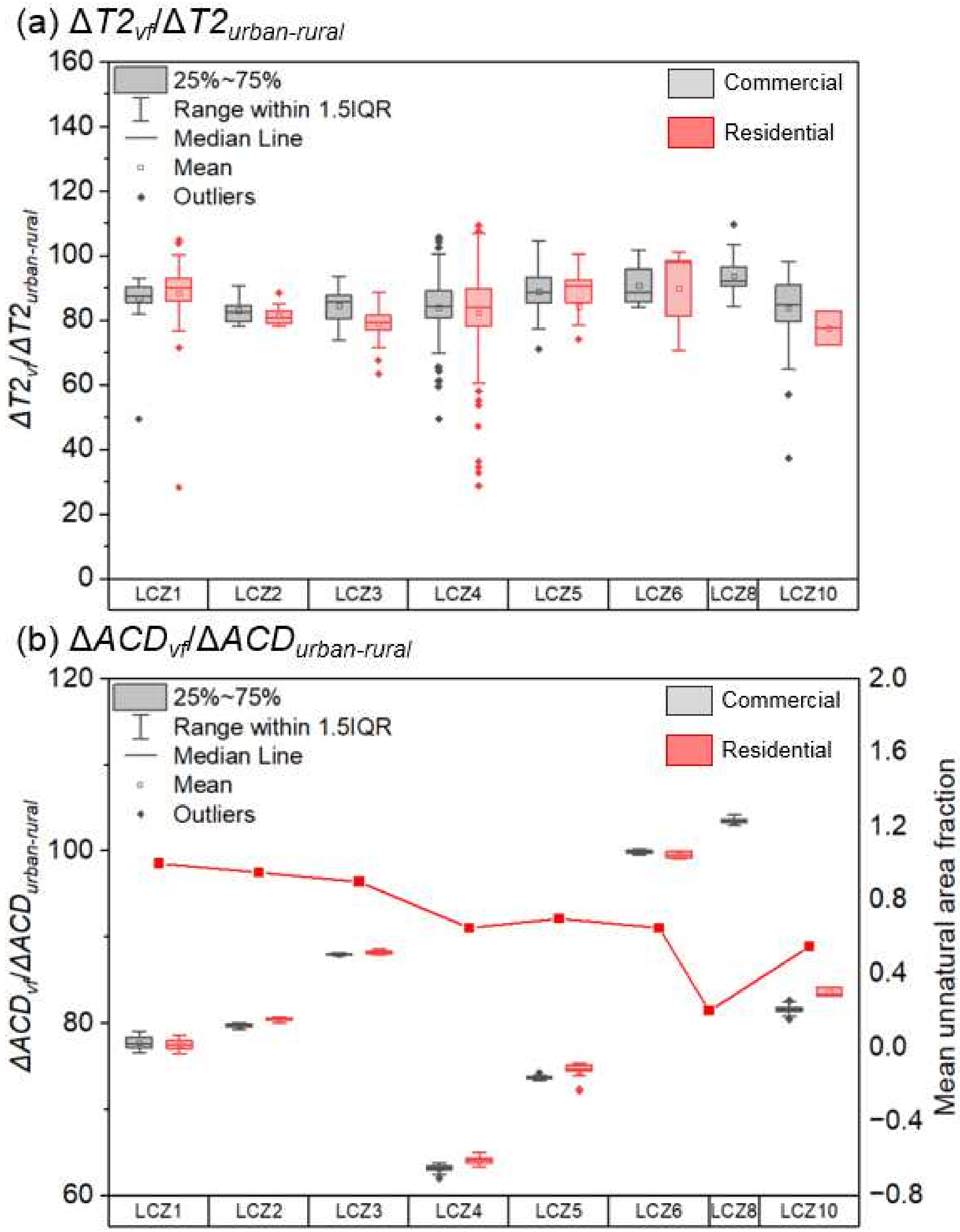

Figure 13. Relative variations of (a) UHIIs ($\Delta T2_{vf}/\Delta T2_{urban\text{-}rural}$) together with (b) air-conditioning load ($\Delta ACE_{vf}/\Delta ACE_{urban\text{-}rural}$) and the mean unnatural area fraction (solid line) plotted as functions of LCZs (boxes).

4.4 Impact of Impervious Surfaces

To investigate the impact of urban-rural impervious surface thermal properties difference ($\Delta ISTP$) on urban climate, the $\Delta ISTP$-induced UHIIs ($\Delta T2_{is}$) are calculated by the temperature difference between real scenario (URBAN-LCZBC) and scenario 4 (RURAL-IMPERVIOUS-SURFACE). Moreover, to quantify the $\Delta ISTP$ contribution to real-urban-rural-climate discrepancy, the relative UHII variations ($\Delta T2_{is}/\Delta T2_{urban\text{-}rural}$) are calculated by Equation (2). Figure 14 shows the diurnal variations of the ensemble averaged $\Delta T2_{is}$ and $\Delta T2_{is}/\Delta T2_{urban\text{-}rural}$ for the LCZBCs. The spatial average of $\Delta T2_{is}$ (0.056 °C) and $\Delta T2_{is}/\Delta T2_{urban\text{-}rural}$ (= 4.75%) are peaked at 1800 LST and 2000 LST, respectively. $\Delta ISTP$ induces gentle UHI at nighttime and urban cool island (UCI) in daytime except the all-day-long UHI in compact high-rise areas (LCZ1). There are mainly two reasons for that: (1) Urban impervious surfaces have a larger heat capacity than rural pavement (Table 2). Given the same incoming solar irradiation, the urban impervious surfaces have a surface temperature cooler than that of rural pavement in daytime while release more heat with a hotter surface temperature at nighttime; (2) Because of their higher thermal conductivity (Table 2), urban impervious surfaces have augmented heat conduction underground that further lowers the surface temperature than that of rural pavement in daytime. On the other hand, the UHI in LCZ1-C is attributed to the dominant low surface albedo. Urban impervious surfaces with lower surface albedo reflect less solar irradiation than does rural pavement that end up with a hotter surface temperature in LCZ 1-C.

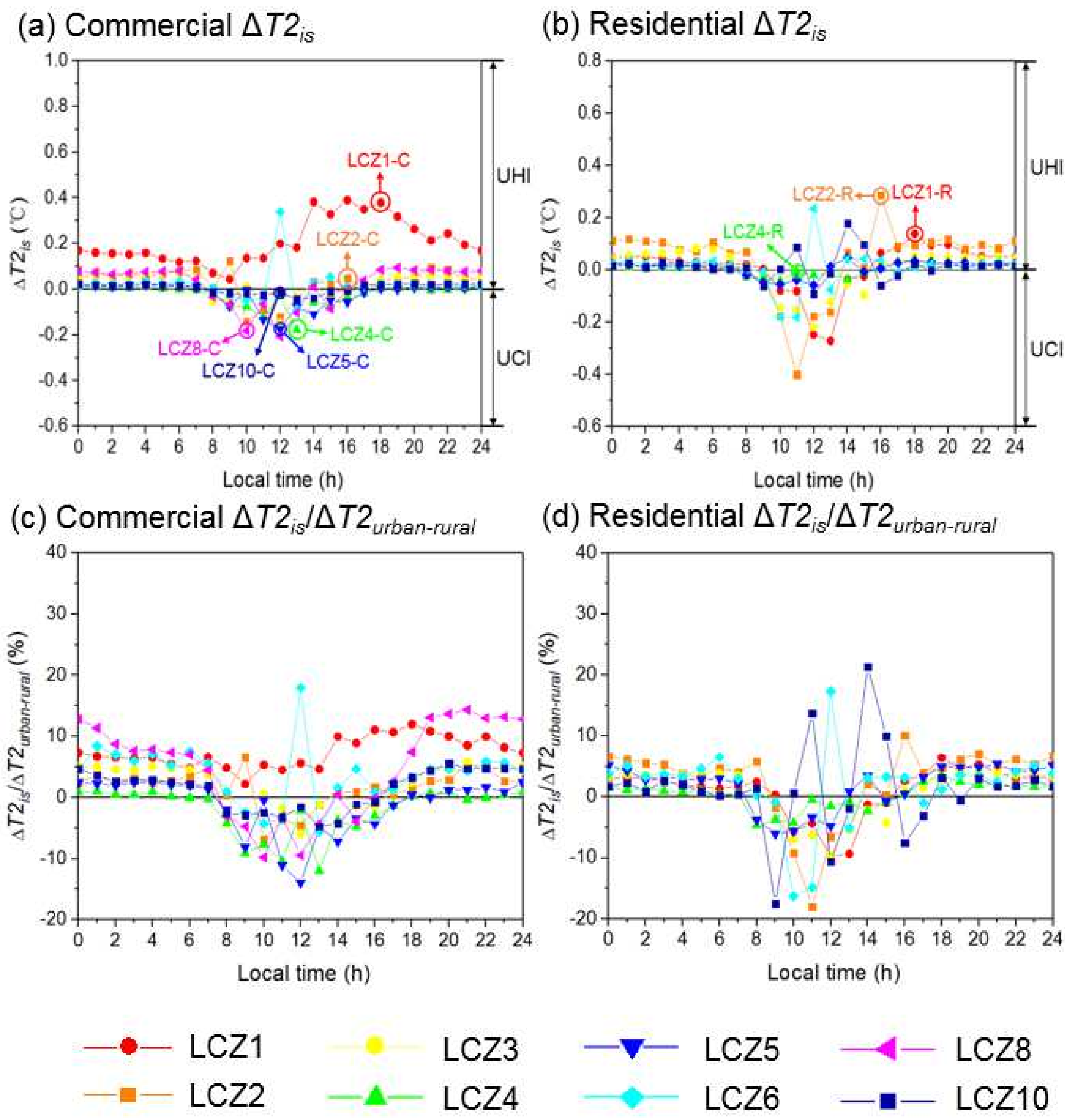

Figure 14. Diurnal variation of ensemble-averaged UHIIs ($\Delta T2_{is}$) induced by urban-rural impervious surfaces thermal properties difference ($\Delta ISTP$) of (a) commercial-dominant and (b) residential-dominant areas together with ensemble-averaged relative variation of UHIIs ($\Delta T2_{is}/\Delta T2_{urban\text{-}rural}$) induced by $\Delta ISTP$ of (c) commercial-dominant and (d) residential-dominant areas for different LCZBCs.

The $\Delta ISTP$ induced sensible cooling demand ΔSCD_{is} is calculated by the temperature difference between the cases UBRAN-LCZBC and RURAL-IMPERVIOUS-SURFACE. Figures 15 a and b depict the diurnal variation of the ensemble averaged ΔSCD_{is} for the LCZBCs. Other than open high-rise (LCZ4-C) and compact high-rise residential (LCZ1-R) areas, $\Delta ISTP$ induces substantial positive ΔSCD_{is} at nighttime but not in daytime for all the LCZBCs. The spatial average of ΔSCD_{is} (= 0.36 w/m^2) is peaked at 0600 LST. The diurnal variation of ΔSCD_{is} is quite consistent with that of $\Delta T2_{is}$ and $\Delta T2_{is}/\Delta T2_{urban\text{-}rural}$. It is thus implied that $\Delta ISTP$ mainly affects building energy consumption by modifying surface temperatures. Besides, the relative variations of additional SCD ($\Delta SCD_{is}/\Delta SCD_{urban\text{-}rural}$) are calculated by Equation (2) to examine the contribution from $\Delta ISTP$ to real-urban-rural-energy discrepancy. Figures 15 c and d show the diurnal variation of the ensemble averaged $\Delta SCD_{is}/\Delta SCD_{urban\text{-}rural}$ for the LCZBCs. $\Delta ISTP$ possesses a key effect at nighttime due to the heat (stored during daytime) is being released. The maximum $\Delta SCD_{is}/\Delta SCD_{urban\text{-}rural}$ is 2.73% at 0600 LST.

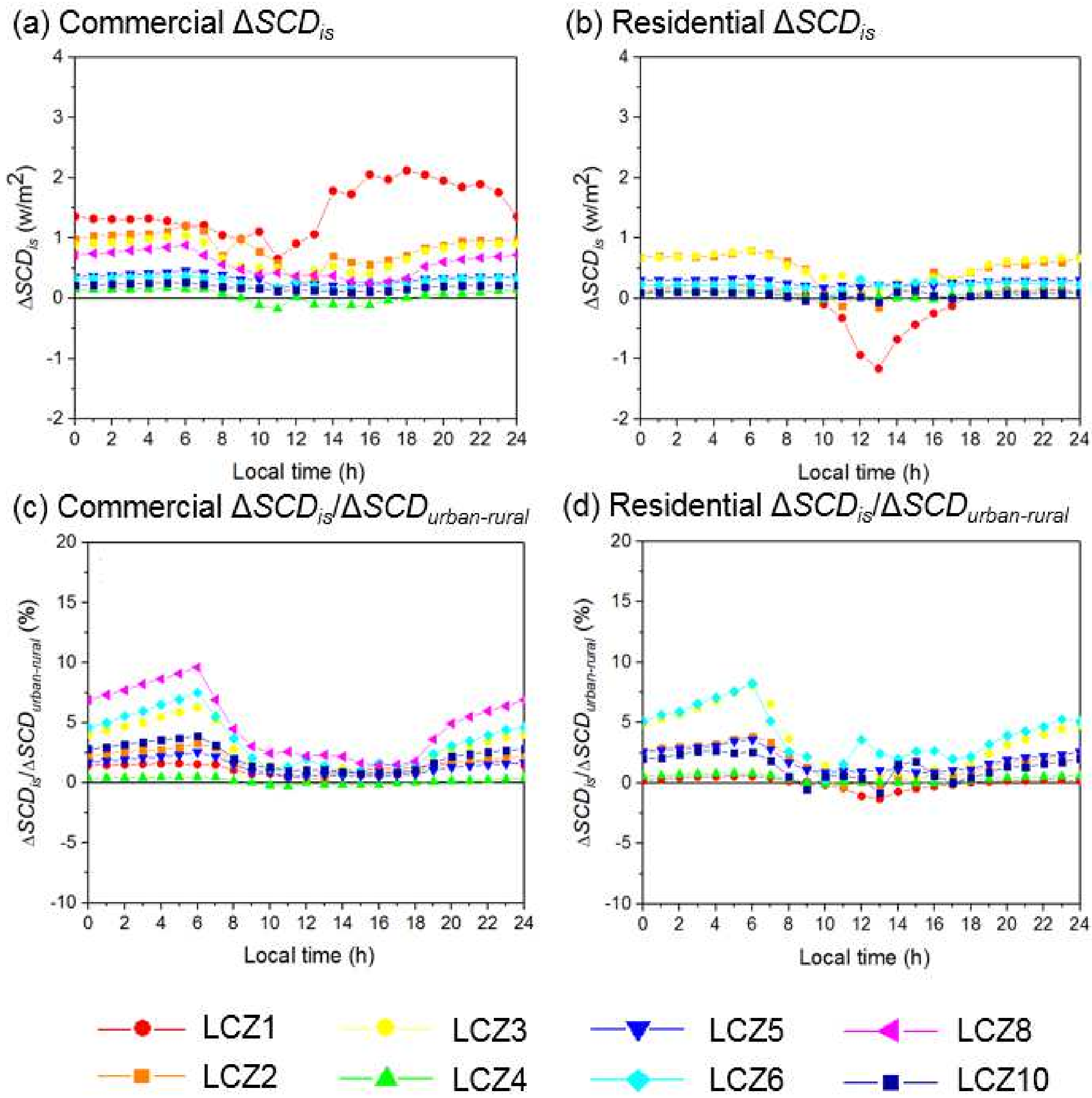

Figure 15. Diurnal variation of ensemble-averaged sensible cooling demand (ΔSCD_{is}) induced by urban-rural impervious surfaces thermal properties difference ($\Delta ISTP$) of (a) commercial-dominant and (b) residential-dominant areas together with ensemble-averaged relative variation of sensible cooling demand ($\Delta SCD_{is}/\Delta SCD_{urban\text{-}rural}$) induced by $\Delta ISTP$ of (c) commercial-dominant and (d) residential-dominant areas for different local LCZBCs.

To compare the effects of $\Delta ISTP$ among different LCZBCs, the daily average of $\Delta T2_{is}/\Delta T2_{urban\text{-}rural}$ and $\Delta ACE_{is}/\Delta ACE_{urban\text{-}rural}$ is calculated (Figure 16). Unlike urban impervious surfaces, rural pavement lowers the building energy consumption in most of the LCZBCs. Moreover, $\Delta T2_{is}/\Delta T2_{urban\text{-}rural}$ and $\Delta ACE_{is}/\Delta ACE_{urban\text{-}rural}$ does not follow the variation of mean impervious surface fraction. Similar to greenery, $\Delta ISTP$ influences building energy consumption by changing surface temperatures. It thus plays a more important role in compact/open mid-rise (LCZ2/LCZ5) and low-rise (LCZ3/6) areas than that in high-rise areas (LCZ1 and LCZ4) with more buildings within the effective height of temperature modulation. Moreover, $\Delta ISTP$ has a major impact on residential-dominant areas than commercial-dominant areas because the energy consumption of residential buildings is more sensitive to ambient temperature (Toparlar et al., 2018; Yang et al., 2020).

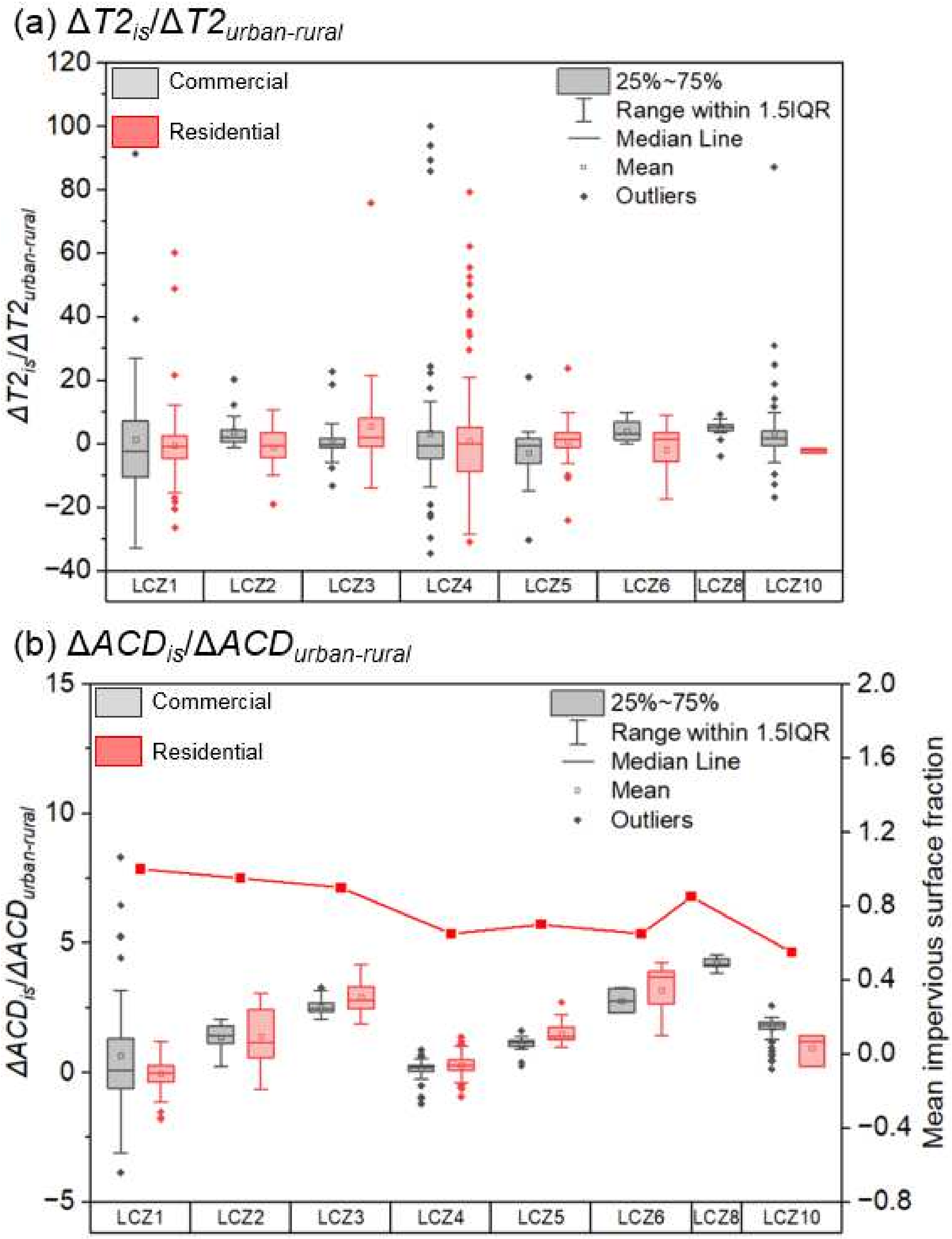

Figure 16. Relative variations of (a) UHIIs ($\Delta T2_{is}/\Delta T2_{urban\text{-}rural}$) together with (b) air-conditioning load ($\Delta ACE_{is}/\Delta ACE_{urban\text{-}rural}$) and the mean impervious surface fraction of different LCZs (solid line) plotted as functions of LCZs.

1

The spatially inhomogeneous urban temperature and AC load caused by heterogeneous LULC types were reported elsewhere. Ortiz et al. (2022) updated the look-up table in WRF based on detailed, spatially heterogeneous UMP data. They calculated the lowest AC load which increases over time in high-rise buildings but the largest increase is found in densely less tall building areas. Xu et al. (2018) used the cooling fraction as a function of urban LULC type to improve the model performance on AC load simulation. The enhancement is significant in nonurban areas but modest in urban areas. These studies have demonstrated the importance of detailed, accurate data for different LULC types. Our current findings show that individual UMPs (e.g. urban structure, VF, or impervious surfaces thermal properties) possess diversified influence on UHII and AC load in commercial and residential areas. It hence signifies the importance of sub-classification to the building categories in the original LCZ types and assign accurate data for each of them.

4.5 Comparison of Urban Morphology Parameters

In this study, the sensitivity of UHII and building energy consumption to urban structure, ΔVF, and $\Delta ISTP$ in real $\Delta ACE_{urban\text{-}rural}$ is studied. UMPs in terms of urban morphology or building categories are more important to AC load than diurnal cycle (Table 8). Figure 17 compares the daily average of relative AC load for different LCZBCs. Urban structure is the integrated variable dominates AC load in compact/open high-rise areas (LCZ1/LCZ4; 81.96%/79.349%). On the other hand, ΔVF is most important in compact/open mid-rise (LCZ2/LCZ5; 80.33%/74.47%), low-rise (LCZ3/LCZ6; 88.17%/99.65%), and large low-rise (LCZ8; 104.11%) areas. In compact/open high-rise areas, heat is trapped at street level due to the high ARs (6 for LCZ1 and 2.75 for LCZ4), weakening the heat removal. Urban structure ends up has a crucial role in Δ*ACE*. However, in compact/open mid-rise (LCZ2/LCZ5) and low-rise (LCZ5/6) areas, Δ*VF* plays a more critical role by modifying the surface temperatures and offering the effective height of temperature modulation. Compared with building redevelopment (18.69 w/m^2), greenery (25.52 w/m^2) is more effective to reduce peaked SCD (Figures 9 and 12). Therefore, it is recommended to reserve more open, greenery space for urban sustainability, especially in compact, commercial-dominant areas. This finding aligns with previous studies in cities with subtropical (Taipei; Yang et al., 2017) and hot-arid (Tehran; Javanroodi et al., 2018) climate.

Table 8. Most important factors in different LCZ and building categories (LCZBCs) together with their contribution to building energy consumption.

LCZBC	Daytime		Nighttime	
	Factor[a]	RVACE [b] (%)	Factor	RVACE (%)
LCZ1-C	US[c]	81.49	US	84.43
LCZ2-C	Δ*VF* [d]	80.55	Δ*VF*	79.41
LCZ3-C	Δ*VF*	88.85	Δ*VF*	87.38
LCZ4-C	US	78.56	US	82.12
LCZ5-C	Δ*VF*	75.59	Δ*VF*	72.71
LCZ6-C	Δ*VF*	100.72	Δ*VF*	98.98
LCZ8-C	Δ*VF*	109.16	Δ*VF*	99.83
LCZ10-C	Δ*VF*	83.63	Δ*VF*	78.71
LCZ1-R	US	78.72	US	82.62
LCZ2-R	Δ*VF*	89.78	Δ*VF*	79.81
LCZ3-R	Δ*VF*	89.40	Δ*VF*	87.35
LCZ4-R	US	75.28	US	80.66
LCZ5-R	Δ*VF*	77.34	Δ*VF*	72.85
LCZ6-R	Δ*VF*	101.27	Δ*VF*	98.06
LCZ8-R	/	/	/	/
LCZ10-R	Δ*VF*	91.04	Δ*VF*	78.80

Remarks:

[a] Factor: The most significant factor

[b] RVACE: Relative variation of AC load

[c] US: The difference in urban-rural building/street structure

[d] Δ*VF*: Urban-rural vegetation fraction difference

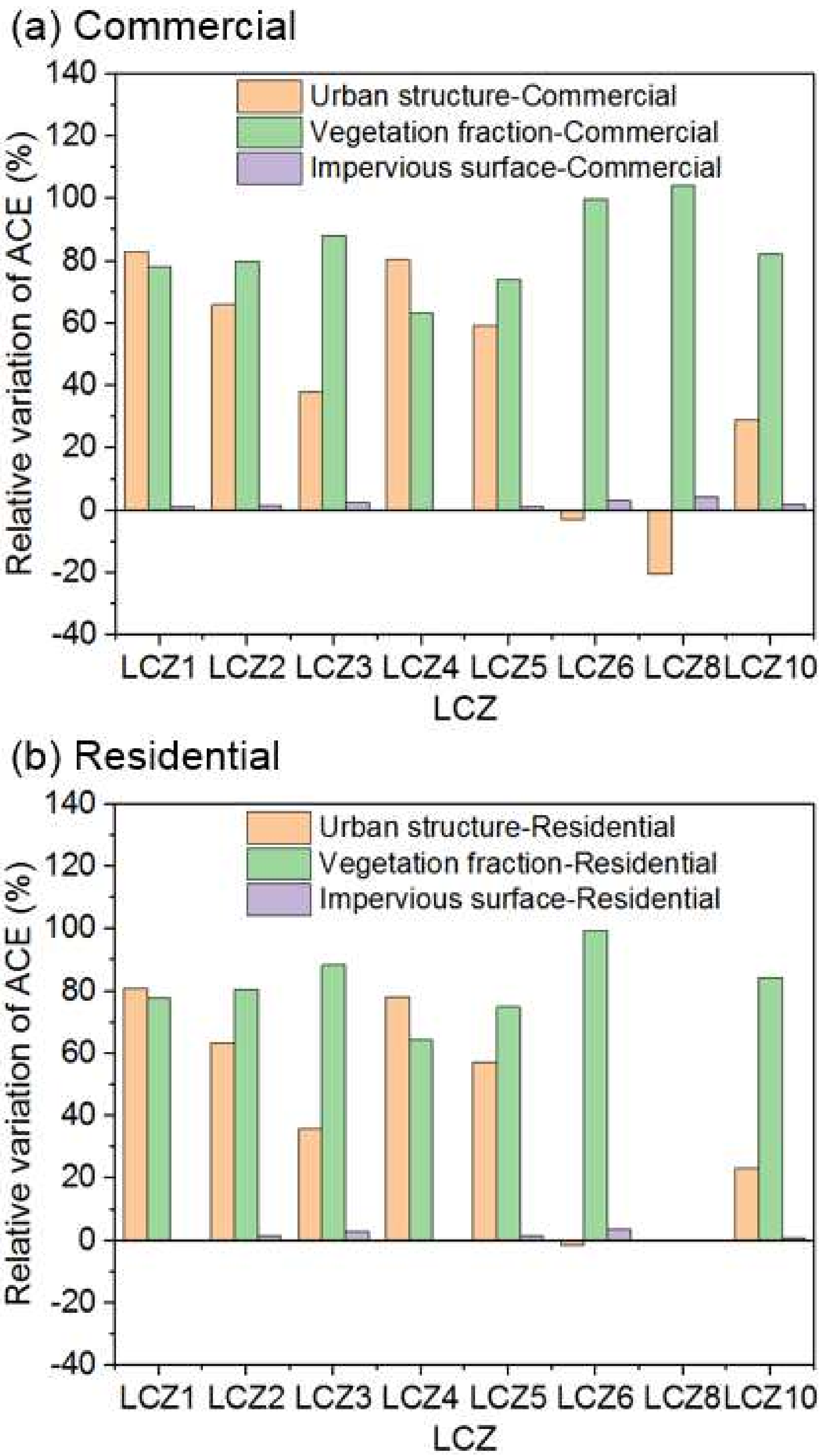

Figure 17. Comparison of relative variation of air-conditioning (AC) load induced by urban structure, vegetation fraction, and urban impervious surface.

The thermal properties of road surfaces are important to ground-level temperature (Mohajerani et al., 2017). Whereas, our results show that their effect on urban thermal environment is rather limited. Different from urban structure and VF, the influence of road surfaces on AC load is negligible. Its impact would be even less in a dense city such as HK where most areas are occupied by buildings rather than roads.

5. Conclusion

In this study, the LCZ and building classification (LCZBC) maps of HK are integrated into a multi-layer WRF-BEP/BEM model for the first time. It is then used to contrast the impact of three UMPs (urban structure, vegetation fraction, and impervious surfaces thermal properties) on the spatio-temporal pattern of UHIIs and building energy consumption during a heatwave event in HK (June 23 to 28, 2016).

Urban structure is found to be the dominant factor in UHIIs at nighttime during which the heat stored during daytime is being released to the atmosphere after sunset. At its peak, the average temperature is increased by 0.59 °C at 0600 LST that contributes 40.33% to UHIIs. Unexpectedly, urban structure could induce the urban cool island in some open (LCZ4 to 6-C/R) and industrial (LCZ10-C/R) areas due to less solar heat gain and higher heat capacity. The difference in vegetation fraction between urban and rural possesses the core impact in daytime (0800-1759 LST) because of the elevated evapotranspiration. The maximum spatial average of temperature increases by 2.08 °C at 1300 LST and the contribution to UHIIs is up to 106.26% at 1000 LST. Greenery consistently mitigates UHI whose benefits are more notable in daytime.

Although they are both induced by urban structure, the diurnal variation of building energy consumption does not follow that of UHIIs. It is because urban structure affects building thermal processes not only by changing ambient temperature but also enlarging the wall/facade areas and heat gain of building envelope. At its peak, SCD is increased by 18.69 w/m^2 at 1600 LST that contributes most (34.52%) to building energy consumption at 0600 LST. On the other hand, greenery consistently reduces building energy consumption by cooling with a maximum SCD increase of 25.54 w/m^2, which portions up to 56.69%, at 1600 LST. Compared with building redevelopment, greenery is more effective to modulate peaked AC load to avoid power grid failure. The influence from urban impervious surfaces is negligible which contributes only 4.75% to UHIIs (2000 LST) and 2.33% to additional SCD (0600 LST). It is noteworthy that the impacts of UMPs on outdoor temperatures lag behind building energy consumption.

The sensitivity of AC load to UMPs for different LCZs and building categories (LCZBCs) is examined in detail. Urban structure is the most important integrated parameter in high-rise building areas, especially for commercial-dominant areas due to the substantial heat trap and intensive anthropogenic heat exhaust. Greenery is found to be most effective to reduce building energy consumption in mid-rise and low-rise areas because more buildings are within the effective height of temperature modulation (less than 10 m). Besides, greenery helps save the building energy in residential-dominant areas where indoor temperatures are more sensitive to the outdoor ones.

The W2W approach used in this study was developed based on the default

(Brousse et al., 2016; Martilli et al., 2016) that is commonly used in WRF modeling (Patel et al., 2022). However, the latest version of W2W tool (Demuzere et al., 2022) based on Python assigns morphological parameters directly to the high-resolution LCZ map which is then aggregated to the lower-resolution WRF grids. It captures well the urban diversity and reduces the uncertainty in urban-canopy parameters. Further efforts are worthy to modify the Python W2W tool and enable it to integrate the LCZBC data (30 urban classes) into the WRF model.

In brief, this study contrasts the roles of urban structure, vegetation fraction, and impervious surfaces thermal properties in local climate and AC load as well as their spatio-temporal characteristics. Next, the most crucial UMP to building energy consumption in individual LCZ types and building categories is identified. The outcome will provide a reference for healthy thermal comfort and sustainable buildings, effectuating environmental policy.

Acknowledgments

This research is conducted in part using the research computing facilities and/or advisory services offered by Information Technology Services (ITS), The University of Hong Kong (HKU). Technical support from Ms. Lilian Y.L. Chan, Mr. W.K. Kwan, Mr. Bill H.T. Yau, and Mr. Juilian Yeung is appreciated. This study is partly supported by the Hong Kong (HK) Research Grants Council (RGC) Theme-based Research Scheme (TRS) T24-504/17-N, the RGC Collaborative Research Fund (CRF) C7064-18G, RGC CRF C5108-20G as well as the RGC General Research Fund (GRF) 17209819 and 17211322. X-X Li acknowledges the support by Guangdong Basic and Applied Basic Research Foundation (Grant No. 2021A1515011890).

References

Alcoforado, M. J., & Andrade, H. (2008). Global warming and the urban heat island. Urban ecology: An international perspective on the interaction between humans and nature, 249-262.

Allen-Dumas, M. R., Rose, A. N., New, J. R., Omitaomu, O. A., Yuan, J., Branstetter, M. L., . . . Adams, M. B. (2020). Impacts of the morphology of new neighborhoods on microclimate and building energy. Renewable and Sustainable Energy Reviews, 133, 110030.

Arghavani, S., Malakooti, H., & Bidokhti, A.-A. A. A. (2020). Numerical assessment of the urban green space scenarios on urban heat island and thermal comfort level in Tehran Metropolis. Journal of Cleaner Production, 261, 121183.

Aslam, A., & Rana, I. A. (2022). The use of local climate zones in the urban environment: A systematic review of data sources, methods, and themes. Urban Climate, 42, 101120.

Assimakopoulos, M., Mihalakakou, G., & Flocas, H. (2007). Simulating the thermal behaviour of a building during summer period in the urban environment. Renewable Energy, 32(11), 1805-1816.

Bougeault, P., & Lacarrere, P. (1989). Parameterization of orography-induced turbulence in a mesobeta--scale model. Monthly weather review, 117(8), 1872-1890.

Brousse, O., Martilli, A., Foley, M., Mills, G., & Bechtel, B. (2016). WUDAPT, an efficient land use producing data tool for mesoscale models? Integration of urban LCZ in WRF over Madrid. Urban Climate, 17, 116-134.

Chan, A. (2011). Developing future hourly weather files for studying the impact of climate change on building energy performance in Hong Kong. Energy and Buildings, 43(10), 2860-2868.

Chen, F., & Dudhia, J. (2001). Coupling an advanced land surface–hydrology model with the Penn State–NCAR MM5 modeling system. Part I: Model implementation and sensitivity. Monthly weather review, 129(4), 569-585.

Chen, H.-C., Han, Q., & de Vries, B. (2020). Urban morphology indicator analyzes for urban energy modeling. Sustainable Cities and Society, 52, 101863.

Chen, L., Ng, E., An, X., Ren, C., Lee, M., Wang, U., & He, Z. (2012). Sky view factor analysis of street canyons and its implications for daytime intra - urban air temperature differentials in high - rise, high - density urban areas of Hong Kong: a GIS - based simulation approach. International Journal of Climatology, 32(1), 121-136.

Crawley, D. B., Lawrie, L. K., Pedersen, C. O., & Winkelmann, F. C. (2000). Energy plus:

energy simulation program. ASHRAE journal, 42(4), 49-56.

Demuzere, M., Argüeso, D., Zonato, A., & Kittner, J. (2022). W2W: A Python package that injects WUDAPT's Local Climate Zone information in WRF. Journal of Open Source Software, 7(76), 4432.

Du, R., Liu, C.-H., Li, X.-X., & Lin, C.-Y. (2023). Effect of local climate zone (LCZ) and building category (BC) classification on the simulation of urban climate and air-conditioning load in Hong Kong. Energy, 271, 127004.

Dudhia, J. (1989). Numerical study of convection observed during the winter monsoon experiment using a mesoscale two-dimensional model. Journal of Atmospheric Sciences, 46(20), 3077-3107.

Friedl, M. A., McIver, D. K., Hodges, J. C., Zhang, X. Y., Muchoney, D., Strahler, A. H., . . . Cooper, A. (2002). Global land cover mapping from MODIS: algorithms and early results. Remote sensing of Environment, 83(1-2), 287-302.

Hong, S.-Y., Dudhia, J., & Chen, S.-H. (2004). A revised approach to ice microphysical processes for the bulk parameterization of clouds and precipitation. Monthly weather review, 132(1), 103-120.

Huang, X., Song, J., Wang, C., Chui, T. F. M., & Chan, P. W. (2021). The synergistic effect of urban heat and moisture islands in a compact high-rise city. Building and Environment, 108274.

Huang, Y., & Niu, J.-l. (2015). Application of super-insulating translucent silica aerogel glazing system on commercial building envelope of humid subtropical climates–Impact on space cooling load. Energy, 83, 316-325.

Hwang, M.-K., Bang, J.-H., Kim, S., Kim, Y.-K., & Oh, I. (2019). Estimation of thermal comfort felt by human exposed to extreme heat wave in a complex urban area using a WRF-MENEX model. International journal of biometeorology, 63(7), 927-938.

Ishii, S., Tabushi, S., Aramaki, T., & Hanaki, K. (2010). Impact of future urban form on the potential to reduce greenhouse gas emissions from residential, commercial and public buildings in Utsunomiya, Japan. Energy policy, 38(9), 4888-4896.

Javanroodi, K., Mahdavinejad, M., & Nik, V. M. (2018). Impacts of urban morphology on reducing cooling load and increasing ventilation potential in hot-arid climate. Applied energy, 231, 714-746.

Ji, J., Chow, T.-T., & He, W. (2003). Dynamic performance of hybrid photovoltaic/thermal collector wall in Hong Kong. Building and Environment, 38(11), 1327-1334.

Jing, R., Wang, M., Zhang, R., Li, N., & Zhao, Y. (2017). A study on energy performance of 30 commercial office buildings in Hong Kong. Energy and Buildings, 144, 117-128.

Kain, J. S., & Fritsch, J. M. (1990). A one-dimensional entraining/detraining plume model and its application in convective parameterization. Journal of Atmospheric Sciences, 47(23), 2784-2802.

Kikegawa, Y., Tanaka, A., Ohashi, Y., Ihara, T., & Shigeta, Y. (2014). Observed and simulated sensitivities of summertime urban surface air temperatures to anthropogenic heat in downtown areas of two Japanese Major Cities, Tokyo and Osaka. Theoretical and applied climatology, 117(1), 175-193.

Lam, J. C., Tsang, C., Li, D. H., & Cheung, S. (2005). Residential building envelope heat gain and cooling energy requirements. Energy, 30(7), 933-951.

Lin, Z., & Deng, S. (2004). A study on the characteristics of nighttime bedroom cooling load in tropics and subtropics. Building and Environment, 39(9), 1101-1114.

Lou, C., Yang, H., Li, Y., & and Cheung, N. h. (2006). Energy audit of buildings: a case study of a commercial building in Causeway Bay of Hong Kong. HV&AC, 2006(36-5), 44-50.

Ma, Y. X., & Yu, C. (2020). Impact of meteorological factors on high-rise office building energy consumption in Hong Kong: From a spatiotemporal perspective. Energy and Buildings, 228, 110468.

Martilli, A., Clappier, A., & Rotach, M. W. (2002). An urban surface exchange parameterisation for mesoscale models. Boundary-layer meteorology, 104(2), 261-304.

Martilli, A., Brousse, O., & Ching, J. (2016). Urbanized WRF modeling using WUDAPT. Paper presented at the Technical Report March, Cientro de Investigaciones Energeticas MedioAmbientales y Tecnologicas (CIEMAT).

Mlawer, E. J., Taubman, S. J., Brown, P. D., Iacono, M. J., & Clough, S. A. (1997). Radiative transfer for inhomogeneous atmospheres: RRTM, a validated correlated‐k model for the longwave. Journal of Geophysical Research: Atmospheres, 102(D14), 16663-16682.

Mohajerani, A., Bakaric, J., & Jeffrey-Bailey, T. (2017). The urban heat island effect, its causes, and mitigation, with reference to the thermal properties of asphalt concrete. Journal of environmental management, 197, 522-538.

Morakinyo, T. E., Ren, C., Shi, Y., Lau, K. K.-L., Tong, H.-W., Choy, C.-W., & Ng, E. (2019). Estimates of the impact of extreme heat events on cooling energy demand in Hong Kong. Renewable energy, 142, 73-84.

Mughal, M. O., Li, X. X., Yin, T., Martilli, A., Brousse, O., Dissegna, M. A., & Norford, L. K. (2019). High‐resolution, multilayer modeling of Singapore's urban climate incorporating local climate zones. Journal of Geophysical Research: Atmospheres, 124(14), 7764-7785.

Oke, T. R. (1982). The energetic basis of the urban heat island. Quarterly Journal of the Royal Meteorological Society, 108(455), 1-24.

Ortiz, L., Gamarro, H., Gonzalez, J., & McPhearson, T. (2022). Energy burden and air conditioning adoption in New York City under a warming climate. Sustainable Cities and Society, 76, 103465.

Ortiz, L. E., Gonzalez, J. E., Gutierrez, E., & Arend, M. (2017). Forecasting building energy demands with a coupled weather-building energy model in a dense urban environment. Journal of Solar Energy Engineering, 139(1), 011002.

Pappaccogli, G., Giovannini, L., Zardi, D., & Martilli, A. (2021). Assessing the Ability of WRF‐BEP+ BEM in Reproducing the Wintertime Building Energy Consumption of an Italian Alpine City. Journal of Geophysical Research: Atmospheres, 126(8), e2020JD033652.

Patel, P., Jamshidi, S., Nadimpalli, R., Aliaga, D. G., Mills, G., Chen, F., . . . Niyogi, D. (2022). Modeling Large‐Scale Heatwave by Incorporating Enhanced Urban Representation. *Journal of Geophysical Research: Atmospheres, 127*(2), e2021JD035316.

Pokhrel, R., Ramírez-Beltran, N. D., & González, J. E. (2019). On the assessment of alternatives for building cooling load reductions for a tropical coastal city. Energy and Buildings, 182, 131-143.

Quan, S. J., & Li, C. (2021). Urban form and building energy use: A systematic review of measures, mechanisms, and methodologies. Renewable and Sustainable Energy Reviews, 139, 110662.

Ren, Z., Fu, Y., Dong, Y., Zhang, P., & He, X. (2022). Rapid urbanization and climate change significantly contribute to worsening urban human thermal comfort: A national 183-city, 26-year study in China. Urban Climate, 43, 101154.

Salamanca, F., Georgescu, M., Mahalov, A., Moustaoui, M., Wang, M., & Svoma, B. (2013). Assessing summertime urban air conditioning consumption in a semiarid environment. Environmental Research Letters, 8(3), 034022.

Salamanca, F., Krpo, A., Martilli, A., & Clappier, A. (2010). A new building energy model coupled with an urban canopy parameterization for urban climate simulations—part I. formulation, verification, and sensitivity analysis of the model. Theoretical and applied

climatology, 99(3), 331-344.
Santos, L. G. R., Singh, V. K., Mughal, M. O., Nevat, I., Norford, L. K., & Fonseca, J. A. (2020). Estimating building's anthropogenic heat: a joint local climate zone and land use classification method. Paper presented at the eSIM Conference 2021.
Shi, L., Luo, Z., Matthews, W., Wang, Z., Li, Y., & Liu, J. (2019). Impacts of urban microclimate on summertime sensible and latent energy demand for cooling in residential buildings of Hong Kong. Energy, 189, 116208.
Siu, L. W., & Hart, M. A. (2013). Quantifying urban heat island intensity in Hong Kong SAR, China. Environmental monitoring and assessment, 185(5), 4383-4398.
Stewart, I. D., & Oke, T. R. (2012). Local climate zones for urban temperature studies. Bulletin of the American Meteorological Society, 93(12), 1879-1900.
Stewart, I. D., Oke, T. R., & Krayenhoff, E. S. (2014). Evaluation of the 'local climate zone'scheme using temperature observations and model simulations. International Journal of Climatology, 34(4), 1062-1080.
Stone Jr, B., Mallen, E., Rajput, M., Gronlund, C. J., Broadbent, A. M., Krayenhoff, E. S., . . . Georgescu, M. (2021). Compound Climate and Infrastructure Events: How Electrical Grid Failure Alters Heat Wave Risk. Environmental Science & Technology, 55(10), 6957-6964.
Takane, Y., Kikegawa, Y., Hara, M., Ihara, T., Ohashi, Y., Adachi, S. A., . . . Kaneyasu, N. (2017). A climatological validation of urban air temperature and electricity demand simulated by a regional climate model coupled with an urban canopy model and a building energy model in an Asian megacity. International Journal of Climatology, 37, 1035-1052.
Toparlar, Y., Blocken, B., Maiheu, B., & van Heijst, G. (2018). Impact of urban microclimate on summertime building cooling demand: A parametric analysis for Antwerp, Belgium. Applied energy, 228, 852-872.
US.EPA. (2007). Guidance on the use of models and other analyses for demonstrating attainment of air quality goals for ozone, PM2. 5, and regional haze. Technical Support Document.
Wang, R., Ren, C., Xu, Y., Lau, K. K.-L., & Shi, Y. (2018). Mapping the local climate zones of urban areas by GIS-based and WUDAPT methods: A case study of Hong Kong. Urban Climate, 24, 567-576. doi:https://doi.org/10.1016/j.uclim.2017.10.001
Wang, Y., Li, Y., Di Sabatino, S., Martilli, A., & Chan, P. (2018). Effects of anthropogenic heat due to air-conditioning systems on an extreme high temperature event in Hong Kong. Environmental Research Letters, 13(3), 034015.
Wang, Z., Xiao, Z., Tam, C.-Y., Pan, W., Chen, J., Hu, C., . . . Yang, S. (2021). The projected

effects of urbanization and climate change on summer thermal environment in Guangdong-Hong Kong-Macao Greater Bay Area of China. Urban Climate, 37, 100866.

Xu, X., Chen, F., Shen, S., Miao, S., Barlage, M., Guo, W., & Mahalov, A. (2018). Using WRF‐Urban to Assess Summertime Air Conditioning Electric Loads and Their Impacts on Urban Weather in Beijing. Journal of Geophysical Research: Atmospheres, 123(5), 2475-2490.

Yang, A.-S., Juan, Y.-H., Wen, C.-Y., & Chang, C.-J. (2017). Numerical simulation of cooling effect of vegetation enhancement in a subtropical urban park. Applied energy, 192, 178-200.

Yang, X., Peng, L. L., Jiang, Z., Chen, Y., Yao, L., He, Y., & Xu, T. (2020). Impact of urban heat island on energy demand in buildings: Local climate zones in Nanjing. Applied energy, 260, 114279.

Yu, C.-R., Guo, H.-S., Wang, Q.-C., & Chang, R.-D. (2020). Revealing the impacts of passive cooling techniques on building energy performance: A residential case in Hong Kong. Applied Sciences, 10(12), 4188.

Yu, Z., Chen, S., & Wong, N. H. (2020). Temporal variation in the impact of urban morphology on outdoor air temperature in the tropics: A campus case study. Building and Environment, 181, 107132.

Electrical and Mechanical Services Department (EMSD) of HKSAR. (2018). Hong Kong Energy End-use Data 2018. Retrieved from https://www.emsd.gov.hk/filemanager/en/content_762/HKEEUD2018.pdf

Electrical and Mechanical Services Department of HKSAR. (2015). Residential air conditioning: an energy efficiency guide. Retrieved from https://www.emsd.gov.hk/filemanager/en/content_718/EMS_Energy(low-res).pdf

Electrical and Mechanical Services Department of HKSAR. (2021). List of Buildings with Stage One Declaration submitted. Retrieved from https://www.emsd.gov.hk/beeo/en/register/search_stageone.php

European Centre for Medium-Range Weather Forecasts. (2016). ERA-Interim datasets. Retrieved from https://www.ecmwf.int/en/forecasts/datasets/reanalysis-datasets/era-interim

Hong Kong Government. (1995). Code of Practice for overall thermal transfer value in Buildings 1995. Retrieved from https://www.bd.gov.hk/doc/en/resources/codes-and-references/code-and-design-manuals/OTTV1995_e.pdf

Hong Kong Government. (2021). Population Estimates. Retrieved from https://www.censtatd.gov.hk/en/scode150.html

Hong Kong Government (2016). Hong Kong Property Review 2016. Retrieved from https://www.rvd.gov.hk/en/publications/hkpr_previous.html

Hong Kong Housing Authority. (2021). Standard Block Typical Floor Plans. Retrieved from https://www.housingauthority.gov.hk/en/global-elements/estate-locator/standard-block-typical-floor-plans/

Hong Kong Observatory. (2022). Information of Weather Station. Retrieved from https://www.hko.gov.hk/en/cis/stn.htm

International Energy Agency. (2019). The Future of Cooling in China. Delivering on action plans for sustainable air conditioning. Retrieved from https://www.iea.org/reports/the-future-of-cooling-in-china

International Energy Agency (2018). The Future of Cooling. Opportunities for energy- efficient air conditioning. Retrieved from https://www.iea.org/reports/the-future-of-cooling

Planning Department of HKSAR. (2012). Urban climatic map and standards for wind environment - Feasibility Study. Retrieved from https://www.pland.gov.hk/pland_en/p_study/prog_s/ucmapweb/ucmap_project/content/reports/executive_summary.pdf

Planning Department of HKSAR. (2018). Land Utilization Map. Retrieved from https://www.pland.gov.hk/pland_en/info_serv/open_data/landu/index.html#!